Universal critical adsorption profile from optical experiments

Andrea J. Liu* and Michael E. Fisher
Institute for Physical Sciences and Technology, University of Maryland, College Park, Maryland 20742
(Received 19 June 1989)

The analysis of optical data for critical adsorption from a fluid (or fluid mixture) onto a wall or interface is discussed theoretically with emphasis on elucidating the universal, scaled adsorption profile $P(z/\xi)$, where $\xi(T)$ is the correlation length and z is the distance from the interface. A novel strategy, which embodies theoretically well-established features, is applied to recent reflectivity and ellipsometry experiments on binary mixtures against glass and vapor substrates. Overall, the data indicate relatively strong surface fields and clearly reveal crossover from a power-law regime, $P(x)\approx P_0/x^{\beta/\nu}$, as $x\to 0$, to $P(x)\approx P_\infty e^{-x}$, as $x\to\infty$, occurring around $x\simeq 1.4$ with $P_\infty/P_0\simeq 0.85$. The relative merits of reflectivity and ellipsometry techniques are assessed (the latter currently proving more definitive) and various experimental issues are identified which must be resolved before more details of the adsorption profile could be extracted from further observations.

I. INTRODUCTION

The phenomenon of critical adsorption occurs when, say, a vapor-liquid, binary liquid mixture, ferromagnet, or other system in the single-phase region is brought to its bulk critical point in the presence of an external wall or other distinct physical interface. In particular, it has often been studied experimentally in binary liquid mixtures in contact with solid substrates and with a vapor interface. Reflectivity and ellipsometry experiments have been reported and will be discussed explicitly below. If one of the components of such an $A+B$ mixture is preferentially attracted to the substrate, it will become partially adsorbed, the composition of the mixture being perturbed over a distance from the substrate of order of the bulk correlation length, $\xi(T)$. To describe the phenomenon in more detail, the order parameter at a distance z from a planar wall, say $m(z)$, is conveniently taken as the deviation of the local volume fraction $\varphi(z)$ of the component which is preferentially adsorbed, say B, from its bulk value $\varphi_B(\infty)$ infinitely far from the wall, that is,

$$m(z)=\varphi_B(z)-\varphi_B(\infty)\ . \tag{1.1}$$

We will generally consider the critical point as being approached as a function only of the temperature T so that $\varphi_A(\infty)$ and $\varphi_B(\infty)$ take their critical values $\varphi_{A,c}$ and $\varphi_{B,c}$. Note that in practice, the volume fractions are somewhat nominal, being defined in terms of number densities $\rho_A^0\equiv N_A^0/V=1/v_A^0$ and $\rho_B^0\equiv N_B^0/V=1/v_B^0$ of *pure* A and *pure* B observed at ambient pressure and some convenient reference temperature. One then has

$$\varphi_A(z)=v_A^0\rho_A(z)/[v_A^0\rho_A(z)+v_B^0\rho_B(z)]\ , \tag{1.2}$$

where $\rho_A(z)$ and $\rho_B(z)$ are the actual local number densities of species A and B in the near-critical mixture.

The functional form of $m(z,T)$ specifies the critical adsorption composition *profile*. Near criticality, the correlation length is the controlling length scale: thus, as $T\to T_c$, one expects the profile to be described in terms of a universal scaling function, as proposed by Fisher and de Gennes in 1978.[1] According to standard scaling arguments, the universal profile should vary algebraically, as an inverse power, near the surface but become exponentially decaying at large distances.[2] Our aim here is to extract more concrete information about the scaling profile from experimental studies of critical adsorption in a systematic way with a minimum of theoretical assumptions. Comparisons between different systems can then be used to test the hypothesis of universality and the scaling functions can be compared with theoretical calculations.

A. Scaling hypothesis

For distances z exceeding molecular dimensions, Fisher and de Gennes[1] proposed that the critical adsorption profile should, asymptotically close to the bulk critical point, follow the scaling law

$$m(z)\simeq m_0 t^\beta P(z/\xi)\ , \tag{1.3}$$

as the reduced temperature deviation from criticality,

$$t\equiv(T-T_c)/T_c\ , \tag{1.4}$$

vanishes. As usual, the exponent β describes the behavior of the coexistence curve below T_c. The shape of the adsorption profile is described by the *scaling function* $P(x)$, which is expected to be universal. The amplitude m_0 sets the magnitude of the physical adsorption. For a nontrivial profile *at* criticality ($t=0$), one must have

$$\text{(A)}\quad P(x)\approx P_0 x^{-\beta/\nu}\ \text{ as } x\to 0\ , \tag{1.5}$$

where ν describes the divergence of the correlation length: see below. It proves convenient to *normalize* the scaling function and remove any arbitrariness in m_0 by setting $P_0\equiv 1$. Away from criticality, on the other hand, the decay must be controlled by the correlation length and one expects[1]

$$\text{(B)}\quad P(x)\approx P_\infty e^{-x} \text{ as } x\to\infty\ , \tag{1.6}$$

provided long-ranged surface-bulk forces may be neglected.[2] Note that the ratio P_∞/P_0 should be universal.

Little more can be said generally about the scaling function, although mean-field theory, which should apply for dimensions $d>4$, predicts $P(x)=1/\sinh x$ with $\beta=\nu=\frac{1}{2}$ so that $P_\infty/P_0=2$. In addition, Bariev[3] has performed exact calculations of $P(x)$ for the semi-infinite two-dimensional square lattice Ising model, where $\beta=\frac{1}{8}$ and $\nu=1$; his results show that $P_\infty/P_0\simeq 1.245\,14$. As regards the experimentally most relevant situation, however, experience suggests that scaling functions in $d=3$ dimensions differ significantly from those in $d=2$ or $d=4$.

In order to analyze the nature of the profile in $d=3$ dimensions on the basis of experimental data, we will first assume that the bulk correlation length $\xi(T)$ at critical composition, is known by direct observation and is well represented in the temperature regime in question by

$$\xi(T)\simeq\xi_0 t^{-\nu}\ . \tag{1.7}$$

Likewise, we propose to accept the well-established theoretical exponent estimates,[4]

$$\nu=0.632\pm0.001 \text{ and } \beta=0.328\pm0.004\ , \tag{1.8}$$

which yield $\beta/\nu=0.519\pm0.007$. Ideally, $\xi(T)$, and thence ξ_0, should be measured by bulk critical scattering experiments; strictly, this yields the second moment correlation length $\xi_1(T)$ which is not identical to that entering in the exponential decay law (1.6) *via* (1.3).[5] However, for three-dimensional systems the difference between ξ_1 and ξ is quite inconsequential at experimental levels of precision.[5] In practice, also, the deviations from (1.7) over the range of interest are unimportant.

For the explicit binary liquid mixtures which we analyze below, the correlation length amplitudes have been determined not by bulk scattering measurements, but by analysis of turbidity experiments on approach to criticality from above T_c, or by measurements of the amplitude of the surface tension as it vanishes on approaching T_c from below. This leaves ξ_0 open to somewhat greater uncertainty than desirable: see details below. Finally, then, the right-hand side of (1.3) may be regarded as known except for the amplitude m_0 and the precise form of the scaling function $P(x)$.

To obtain a tractable scheme of analyzing the experimental data, we postulate acceptable forms for $P(x)$ containing one or more parameters. Various such explicit models for the scaling function $P(x)$ are listed below in Sec. I D; one simple but fully adequate example is

$$P(x)=\left[\frac{1+cx}{x}\right]^{\beta/\nu} e^{-x}\ . \tag{1.9}$$

This function varies algebraically as $x^{-\beta/\nu}$ ($P_0\equiv 1$) for small x and exponentially as e^{-x} for large x, in accord with the scaling predictions laid out above. Evidently, the crossover from algebraic to exponential decay is tuned by the parameter c, which we expect to be of order unity. Note that for small c, the crossover occurs at large x, so the algebraic region is large. That is a specific feature we may hope to resolve on the basis of experiments. The universal ratio mentioned above takes the value $P_\infty/P_0=c^{\beta/\nu}$. Plots of this profile for various choices of c appear in Fig. 1.

B. Reflectivity and ellipsometry

We have examined critical adsorption data for three different binary mixtures obtained from reflectivity and ellipsometry experiments. The reflectivity observations were made by Schlossman, Wu, and Franck[6] (SWF) on the binary mixture of nitromethane-carbon disulfide ($CH_3NO_2+CS_2$) against a glass substrate. The ellipsometry data were made available to us by Schmidt and Moldover[7] for the mixture isopropanol-perfluoromethylcyclohexane (i-$C_3H_7OH+C_7F_{14}$), and by Schmidt[8] for the mixture methylcyclohexane-perfluoromethylcyclohexane ($C_7H_{14}+C_7F_{14}$) against their respective vapor-liquid interfaces.

The reflectivity R is simply the ratio of the intensities of light incident on and reflected by the glass-liquid interface at a given angle of incidence θ_1. In the mixture studied, the index of refraction of the nitromethane, which is preferentially adsorbed, is less than the index of refraction of the glass. Thus, the reflectivity increases as the amount of nitromethane adsorbed increases. According to elementary optics, the reflectivity measures the deviation of the index of refraction in the mixture from that of the substrate. Far from the wall, the index of refraction approaches its bulk value for the binary mixture of criti-

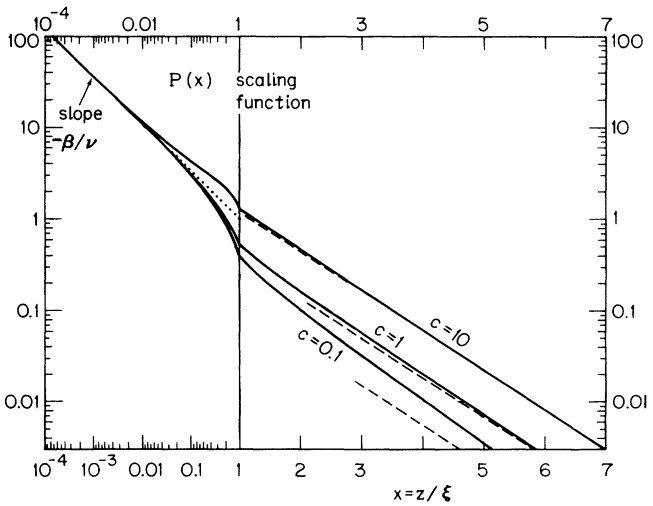

FIG. 1. Plots of the model scaling function (c) [see (1.9) and (1.14)] for the critical adsorption profile for three choices of the parameter c. Note the break in the x scale from logarithmic to linear at $x=1$ (corresponding to $z=\xi$), indicated by a vertical line. Evidently, c controls the location and nature of the crossover from power-law behavior for small x (dotted linear asymptote on the log-log plot) to exponential decay for large x (dashed linear asymptotes on the semi-log plot). Our analysis indicates that the smaller values, $0.1\le c\le 1$, give the best fits to the reflectivity and ellipsometry data: see the text.

cal composition and given temperature. Since adsorption occurs only within several correlation lengths of the surface, which is generally much less than the wavelength of incident light, most of the contribution to the total reflectivity arises from the bulk. This large "background" value, say R_b, must be allowed for in analyzing the measured reflectivity R to extract the reflectivity increment ΔR actually attributable to the critical adsorption. Thus, as we shall see in Sec. II C, observations of ΔR are highly sensitive to uncertainties in the measured or estimated value of the bulk index of refraction.

One must also recall that a reflectivity experiment actually measures the deviation of the dielectric constant (or refractive index) from its bulk value; one may assume that the composition profile is linearly proportional to the dielectric constant profile, or in other words, that the Lorentz-Lorenz relation is valid.[9] However, we will sidestep this issue to some degree by working primarily with the dielectric constant profiles. Some explicit profiles for the mixture of SWF deduced from our fits are drawn in Fig. 2.

Ellipsometry experiments, on the other hand, measure the ratio of the complex Fresnel reflection amplitudes r_s and r_p for s- and p-polarized light, respectively. (We recall that s-polarized light is linearly polarized with the electric field perpendicular to the plane of incidence, while p-polarized light is also linearly polarized, but with the magnetic field perpendicular to the plane of incidence). The ratio can be expressed as

$$r_p/r_s = e^{i\Delta}\tan\psi \ , \tag{1.10}$$

where the magnitude is written as $\tan\psi$ for convenience. The coefficient of ellipticity, $\bar{\rho}$, is defined as the ratio of the minor and major axes of the ellipse of polarization. If light is incident at the Brewster angle $\theta_1 = \theta_B$, then $\Delta = \pi/2$ by definition, and

$$\bar{\rho}_B \equiv \mathrm{Im}(r_p/r_s) \ . \tag{1.11}$$

This is the quantity actually measured by Schmidt and Moldover.[7,8] In the case of a slab profile, i.e., an ideal sharp step from the index of refraction of the substrate to that of the bulk fluid, $\bar{\rho}_B$ vanishes. Hence, the experiment directly measures the deviation from a sharp step. Evidently, one advantage of ellipsometry over reflectivity is that it is insensitive to the index of refraction of the bulk fluid, the observed response depending wholly on the adsorption profile and the structure of the substrate-liquid interface. As regards critical adsorption, however, the situation is not quite so simple since, as mentioned, one is interested in relatively large scales of order $\xi(T)$, while the ellipticity is sensitive also to the behavior of the profile on molecular scales; fortunately, the corresponding background proves less important than in the case of reflectivity.

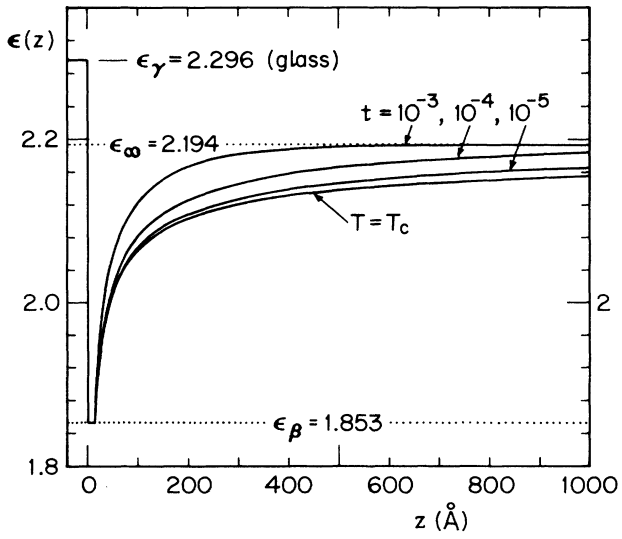

FIG. 2. Variation of the dielectric constant profile for nitromethane preferentially adsorbed on a glass wall (occupying $z \le 0$) from a near critical mixture with carbon disulfide. The plots derive from a representation using the scaling function form (c) [Eq. (1.9)] with $c = 0.1$ which is reasonably consistent with the reflectivity data over the range $t = 10^{-2}$ to 10^{-5}. Note that at least one layer of nitromethane is predicted to be adsorbed against the glass.

C. Strategy for analyzing experimental data

Experiments on critical adsorption have also been performed using the techniques of fluorescence,[10] and of gravimetry and volumetry,[11,12] in addition to reflectivity[6,13] and ellipsometry.[7,8,14–16] The main difficulty with extracting profile information from these experiments is that most techniques measure only some integral over the profile but do not otherwise provide spatial resolution. In the case of volumetric and gravimetric techniques, where the spatial resolution is determined by the size of the probe, this is unavoidable. It is difficult to envision how small enough probes could be fashioned to measure details of the profile. A qualitative exception is the elegant technique developed by Beysens and Leibler,[10] which uses fluorescence by an evanescent wave to measure the adsorption. By varying the incident angle one can vary the distance probed by the evanescent wave. Thus, one can directly observe the fluorescence increase closer to the wall. In order to relate the fluorescence to the profile quantitatively, however, one must integrate Maxwell's equations over the profile. Thus, the quantitative analysis for such an experiment is basically no simpler than it is for optical experiments.[17]

Optical experiments such as reflectivity and ellipsometry also measure integrals of the solutions of Maxwell's equations over the profile. Thus in order to gain information about the profile, one is forced to postulate some profile and integrate Maxwell's equations numerically to compare the predicted reflectivity or ellipticity with the measured data. Some authors have used the Born approximation to deconvolute data more directly but it turns out that this is inadequate for both reflectivity and ellipsometry, as we discuss in more detail in Secs. II and III. The strategy adopted here is to consider various model profiles predicted by a scaling function $P(x)$ with no free parameters. Then, as explained, the physical profile $m(z)$ is completely specified up to an overall amplitude factor m_0: see (1.3). For each data

point taken at a measured temperature (and angle θ when this is varied), the experimentally observed reflectivity or ellipticity is fitted by adjusting only m_0. This results in an *effective amplitude function*, $\tilde{m}_0(t)$. If the model were indeed correct, or sufficiently close to reality, $\tilde{m}_0$ would be independent of t (and of θ). In practice, one might hope for constancy within the experimental noise and error bars. Any systematic temperature dependence in $\tilde{m}_0(t)$ indicates an unsatisfactory choice of $P(x)$, or possibly, deviations from scaling behavior, or, more likely than the failure of scaling, some problem with the various adjustments to the data, such as the background subtraction. If, however, one trusts scaling and can control the data corrections, the variation of $\tilde{m}_0(t)$ yields definite quantitative information on the shape of the profile, as we will demonstrate.[18]

The "goodness of fit" for each profile may be measured by the fractional deviation of $\tilde{m}_0(t)$ over the temperature range covered by the experiment. For SWF this is $10^{-5} \lesssim t \lesssim 10^{-3}$ i.e., two decades close to T_c. For the ellipticity measurements[7,8] one has $10^{-4.5} \lesssim t \lesssim 10^{-1.5}$. The fitted parameter $\tilde{m}_0$ clearly contains absolute information since it directly measures a physical quantity, namely, the local dielectric constant or volume fraction. To compare different profiles quantitatively, however, it may be convenient to rescale $\tilde{m}_0(t)$ so that its reduced value is unity at a convenient reference temperature.

The model scaling profiles we have considered are listed in Sec. I D. For simplicity we sometimes adopt the approximation $\beta/\nu=\frac{1}{2}$ (in place of $\beta/\nu=0.519$; see above). We found, for the SWF data, that this made at most 3% to 6% differences in the value of $\tilde{m}_0$ for a given form of profile; this proved unimportant relative to the noise levels and residual trends with t: see Sec. II.

D. Model scaling profiles

It proves instructive to explore the theoretically crudest profile shapes if for no other reason than to see if the experiments can actually discriminate against them! Thus we have examined the following models.

(a) *Slab form:*

$$P(x)=\begin{cases}1 & \text{for } x \le 2\\ 0 & \text{for } x>2\end{cases}. \tag{1.12}$$

This of course, violates both conditions A and B above, (1.5) and (1.6). The cutoff at $x=2$ yields a first moment of unity, as does the next profile.

(b) *Pure exponential form:*

$$P(x)=e^{-x}, \tag{1.13}$$

as used by SWF at one stage of their analysis. This satisfies condition B but violates the critical point decay law condition A (unless $\beta=0$ which describes Ising-like criticality only for $d=1$ with $T_c=0$) so that the ratio P_∞/P_0, defined after (1.6), diverges.

The violation of condition A has a particular, unrealistic physical consequence worth emphasizing. Specifically, if $P(x)$ remains bounded as $x\to 0$, the scaling form (1.3) predicts that the value of the order parameter $m(z)$ at fixed z, say near the wall, eventually *decreases* as $T\to T_c$ and *vanishes* at $T=T_c$. Such a decrease of $m(z)$ as $T\to T_c$, even though the integral $\int_0^\infty m(z)dz$ diverges like $1/t^{\nu-\beta}\simeq 1/t^{\nu/2}$, seems quite unphysical. Indeed, not only does it contradict mean-field theory, but for models like the nearest-neighbor ferromagnetic Ising model, it also violates the rigorous GKS inequalities.[19] [In principle, however, sufficiently strong corrections to scaling might restore the expected monotonic increase of $m(z)$ at fixed z as $T\to T_c+$; on the other hand, requiring the scaling form to imply monotonicity imposes the condition $-d\log P(x)/d\log x>\beta/\nu$, which probably should be respected.]

(c) *Power-law–exponential form:*

$$P(x)=\left[\frac{1+cx}{x}\right]^{\beta/\nu} e^{-x}. \tag{1.14}$$

This model, reproduced again here for completeness, meets both conditions A and B, as do the subsequent models. However, if $m(z;T)$ is to be monotonic in T at fixed z, one should have $c\le \nu/\beta$.

(d) *Hyperbolic sine form:*

$$P(x)=\left[\frac{\beta}{\nu}\sinh\frac{\nu}{\beta}x\right]^{-\beta/\nu}. \tag{1.15}$$

This elegant form was originally proposed by Peliti and Leibler,[20] with $\beta/\nu=\frac{1}{2}$, on an *ad hoc* basis. It implies $P_\infty/P_0=(2\nu/\beta)^{\beta/\nu}\simeq 2.01$. Monotonicity in T at fixed z is ensured.

(e) *Exponential–Padé form:*

$$P(x)=\left[\frac{1+c(1-e^{-x})}{1-e^{-x}}\right]^{\beta/\nu} e^{-x}. \tag{1.16}$$

This form, and its extensions found by adding further integral powers of e^{-x} in the numerator and denominator of the prefactor, gives added flexibility over the hyperbolic sine profile (d), and, in preference to (c), gives a decay-law generalizing condition B as

$$m(z)=P_\infty e^{-x}+P'_\infty e^{-2x}+P''_\infty e^{-3x}+\cdots, \tag{1.17}$$

with $P_\infty/P_0=(1+c)^{\beta/\nu}$. It seems likely that, as mean-field theory and Bariev's work[3] indicate, the scaling function for large x should have such an expansion rather than one involving inverse powers of x times an exponential, as implied by (1.14).[21]

In the case of an experiment measuring adsorption against a wall, the dielectric constant profile $\epsilon(z)$ can be constructed from $m(z)$ with the aid of (i) the dielectric constant $\epsilon_\infty(T)$ of the bulk mixture far from the wall, (ii) a scale factor, say ϵ_0, for deviations from the bulk, (iii) a cutoff value ϵ_β corresponding to the pure component B, and (iv) the dielectric constant, say ϵ_γ, of the wall material or phase γ: see Fig. 2. In the situation $\epsilon_\beta<\epsilon_\infty$, which corresponds to the experiments of SWF, we may thus take

$$\epsilon(z)=\begin{cases}\epsilon_\gamma & \text{for } z<0\\ \max\{\epsilon_\beta;\epsilon_\infty-\epsilon_0 m(z)\} & \text{for } z>0\end{cases}. \tag{1.18}$$

Of course, the Lorentz-Lorenz factor ϵ_0 might well be absorbed into the value of m_0 for the purposes of fitting.[22]

Now, as mentioned, a reflectivity measurement is not sensitive to the precise variation of $\epsilon(z)$ near the wall, especially if, as in SWF's experiments, the dielectric constant ϵ_γ, corresponding then to glass, does not differ greatly from ϵ_∞ or ϵ_β. Thus the sharp discontinuity in $\epsilon(z)$ at $z=0$ implied by (1.18) is adequate for that situation. On the other hand, the ellipsometry experiments used to study adsorption on a vapor interface[7,8] are sensitive to details of the liquid-vapor interface which, furthermore, must have structure on the vapor side controlled by the finite, but non-negligible correlation length, say $\xi_\gamma(T)$, of the vapor (or γ) phase. Appropriate models for the dielectric constant profile right through the interface in this case must, therefore, be constructed with more attention to the details close to the interface. This issue is addressed in Sec. III B.

E. Summary of conclusions

The method of analysis sketched in Sec. I D above proves quite sensitive. Using the reflectivity data of SWF for nitromethane-carbon disulfide, we are first able to see that the slab profile, (a) above, and the pure exponential profile (b) provide distinctly worse representations of the experiments than do profiles with the expected power-law behavior for small scaled variable x. Indeed, by varying the parameter in the power law–exponential form (c) and comparing also with the model profiles (d) and (e), one finds that if, for a given t, the power-law region extends to larger values of z before the exponential behavior takes over, the goodness of fit is improved. Values of the ratio P_∞/P_0 in the range 0.2 to 1.0 are suggested. However, to the extent that the analysis has been carried, we always find significant, *systematic, residual deviations* of $\tilde{m}_0(t)$ from constancy. As explained below, we believe these are associated with uncertainties in the determination of T_c and with an inability, using existing data, to establish $\epsilon_\infty(T)$ and thence the background reflectivity R_b, with sufficient precision. In default, at present, of a way of determining the background with greater confidence and less ambiguity, it is not worthwhile to pursue the more elaborate forms of profile (e), etc., in an effort to reduce or, possibly, to eliminate the systematic deviations. More extensive and precise experimental data should, however, enable one to resolve the nature of the profile to a significantly higher degree.

Despite the current limitations, one finds that all the power-law profiles attain *saturation* in the sense that $\epsilon(z)\equiv\epsilon_\beta$ holds over a region of about 15 Å near the wall: see Fig. 2. That suggests that in the real system the wall is essentially covered with a layer of pure B ($\equiv$nitromethane) of thickness one or more monolayers. This is consistent with a strong short-ranged interaction between the adsorbed component, nitromethane, and the glass, acting at the glass substrate. The interaction is, in actuality, believed to be the result of hydrogen bonding,[6] which is indeed strong (of the order of k_BT per bond) relative to van der Waals or dipole-dipole interactions.

Now the fuller scaling theory for short-ranged wall interactions entails a surface field H_1, measured, say, in energy units per molecule. The experimental data thus indicate that $h_1\equiv H_1/k_BT_c$ is of order unity or larger. However, the reflectivity data *per se* cannot give an unambiguous estimate of the on-wall composition since replacing z by $z-z_a$ (for $z>0$) in (1.18) changes the profile drastically near the wall but will have no significant effect on the reflectivity provided $z_a\ll\lambda$ where λ ($=6328$ Å) is the wavelength of incident light. By the same token, one cannot hope to determine H_1 with significant accuracy.

The scaling theory for general h_1 actually replaces the form (1.3) by[23]

$$m(z)=m_0t^\beta P(z/\xi,h_1/t^{\Delta_1}) , \tag{1.19}$$

where the surface exponent Δ_1 is close to 0.5. (From the estimate[23] $\beta_1=0.79\pm0.01$ for Ising-like systems and the hyperscaling relation $\beta_1=2\nu-\Delta_1$, one obtains $\Delta_1=0.47_4\pm0.01$.) If critical adsorption is observed at all, one should have $h_1\neq0$. Then, since Δ_1 is positive, h_1/t^{Δ_1} diverges as $t\to0$ and so the *strong surface-field limit,* with scaling function $P(x)=P(x;\infty)$, should apply close enough to T_c. Since h_1 seems to be of order unity, this scenario would seem to be fully applicable for the nitromethane-carbon disulfide mixture on a glass wall in SWF's experiments.

The ellipsometry data of Schmidt and Moldover[7] on the vapor-liquid interface of isopropanol-perfluoromethylcyclohexane prove difficult to analyze conclusively; however, our analysis of these data and those[8] for methylcyclohexane-perfluoromethylcyclohexane also clearly discriminates against the slab and pure exponential profiles, (a) and (b) in Sec. I D. Furthermore, there is a good evidence of algebraic decay in the profile close to criticality, crossing over to exponential decay at values of z/ξ roughly in the range 1.2 to 1.7. In the case of nitromethane-carbon disulfide against glass, on the other hand, we could only conclude that the crossover lay in the wide range 1.0 to 20. This might, perhaps, be interpreted as suggesting a more extended algebraic region which would, then, violate expectations of universality. However, the data are certainly consistent with the universality of $P(x)$ across all three systems.

Although the significance of various systematic errors and data corrections discussed below must not be underrated, a possible source of nonuniversality in $P(x)$ might lie in the dependence of the profile on the surface field H_1. If $h_1\equiv H_1/k_BT_c$ were small for the vapor interface, which is not *a priori* implausible, it may be that the temperature regime probed by the experiments (roughly $5\times10^{-5}<t<0.05$) is not sufficiently close to T_c for h_1/t^{Δ_1} to become large enough to justify the use of (1.3) with $P(x)\simeq P(x;\infty)$. Indeed, the vapor interfaces may lie in a crossover region between weak and strong surface fields. Such a situation has been discussed quantitatively by Nakanishi and Fisher[24] for the shift in critical temperature of a fluid confined between parallel plates. Further weight is lent to such a rationalization if one inquires into the origin of the surface interactions. The adsorbed component B ($\equiv$perfluoromethylcyclohexane) has an index of

refraction which lies between that of the vapor and of methylcyclohexane. According to the theory of dispersion forces,[25] this is the preferred configuration if the controlling interactions are of van der Waals character. Although the short-ranged part of the van der Waals interaction and an effective H_1 are hard to estimate, it seems likely to be significantly weaker than the hydrogen bonding operative at the liquid-glass interface. Further experimentation and analysis, however, are really needed to establish whether the results truly differ between the two systems and to demonstrate that small h_1 is then the cause of this difference.

The ellipsometry data indicate values of the universal ratio P_∞/P_0 in the range 0.75 to 0.95 for profile (c) but somewhat large, 0.9 to 1.1, for the profile (e) in Sec. I D; the lower values overlap the wider span of 0.2 to 1.0 suggested by the reflectivity data. As a combined estimate based on all three sets of data, we have adopted $P_\infty/P_0 \simeq 0.85$. It may be remarked that this estimate does not lie between the values predicted for $d=2$ and for $d>4$, namely $P_\infty/P_0 \simeq 1.245$ and $P_\infty/P_0 = 2$. Although there is no *a priori* reason why P_∞/P_0 must be monotonic as a function of dimensionality, many critical parameters are found to be so; hence our result is, perhaps, unsettling. One should notice, however, that fits based on generalizations of the exponential Padé profile (e) involving more than one parameter, might well yield still higher values of P_∞/P_0; we have not employed such more elaborate model profiles here because they are not warranted by the presently available data. One may be optimistic, however, that future experiments, which pay attention to various sensitive experimental issues that our analysis has revealed (see Sec. IV), will be able to resolve the behavior of the adsorption profile in more definitive detail.

F. Organization and caveats

The rest of this paper is divided into three parts. Section II reviews the reflectivity experiment[6] and presents the detailed results of our analysis of the SWF data. We show explicitly that the Born approximation is inadequate for calculating the reflectivity as, indeed, has been argued by Beaglehole.[26] In addition to the theoretical conclusions summarized above, our analysis pinpoints several experimental problems which must be resolved before more detailed profile information can be extracted from reflectivity data of the sort currently available. Section III is devoted to ellipsometry. The experiments[7,8] are briefly reviewed; then the specific model dielectric constant profiles, which encompass the vapor phase γ, are discussed. As explained, these incorporate the universal scaled profiles of (1.3) and Sec. I D, but are more elaborate since they must represent a smooth transition through the interface into the vapor, which is assumed to be described by a hyperbolic tangent or Fisk-Widom[27] profile. Various ways of matching a critical adsorption profile onto the vapor profile have been studied and the most useful are described. The validity of the Born approximation is examined. The results of the ellipsometry analysis are summarized, and experiments are suggested which would yield additional information.

Finally, the two experimental techniques are compared in Sec. IV, and their shortcomings and associated effects on our analysis are discussed. Other concerns are also mentioned, in particular, the effect of van der Waals forces and critical opalescence. The former are irrelevant to bulk criticality and also, in a renormalization group sense, to critical adsorption.[20] However, as emphasized by Dietrich and Schack,[28] van der Waals interactions do give rise to z^{-3} tails in the profiles, which we do not take into account. In principle, this might be worth allowing for; however, we present semiquantitative arguments indicating that the effects are unlikely to be significant for the experiments of the sort analyzed here. (See also the Appendix). It should also be mentioned, in this connection, that Dietrich and Schack[28] have presented a detailed discussion of the analysis of reflectivity data for situations where a power-law adsorption profile is anticipated, as, in our case, at $T=T_c$. They find that neutrons and hard x rays are much preferable to light. Their analysis, insofar as it applies only at $T=T_c$, may be regarded as complementary to ours, which focuses on the approach to criticality.

The second concern regarding critical opalescence poses a more difficult problem. An essential assumption of our analysis (and of all previous discussions) is that the local index of refraction varies only in the direction perpendicular to the substrate, so that one may integrate Maxwell's equations only along the normal to the substrate. However, diverging critical composition fluctuations necessarily lead to fluctuating nonuniformity parallel to the plane of the interface. This issue has been discussed recently by Bedeaux, Blokhuis, and Schmidt.[29] Although the quantitative importance of the effect has not yet been fully elucidated, these authors conclude that the contribution to the ellipticity of a critical interface due to transverse fluctuations probably becomes unimportant close to the critical point. The implication of these effects for critical adsorption (entailing a *noncritical* interface or wall) remains an open question. Nevertheless, it is plausible that they do result in some renormalization of the scaled dielectric constant profile (which is what the experiments really "see") relative to the mean composition profile.[22]

II. REFLECTIVITY EXPERIMENTS

A. Some experimental details

In their experiment, Schlossman, Wu, and Franck[6] reflected a HeNe laser beam with $\lambda = 6328$ Å from the interface between an optical glass prism and the binary liquid mixture. Nitromethane (B) and carbon disulfide (A) were prepared in proportions within 1% of the critical composition, $\phi_{A,c} = 0.601$. The glass prism constitutes the bottom wall of the cell containing the fluids, and was subject to chemical cleaning designed to leave hydroxyl (OH) groups on the surface: this wall preferentially attracted the polar nitromethane molecules.[13]

The incoming light was set at a fixed angle of incidence

$\theta_1 = 77.6°$, close to the angle of total internal reflection, which, close to T_c, is $\theta_c = 77.85°$. An apparent advantage of choosing an angle near θ_c is that the reflected intensity is highest there; but, on the other hand, the length scale probed increases as θ_1 approaches more closely towards θ_c. The reflectivity at such high angles is therefore less sensitive to the shape of the profile near the wall, and depends mostly on the tail of the profile, which is always exponential. We believe that better results can probably be obtained at smaller angles. More generally, it would be advantageous to measure the reflectivity at a number of different angles in order to gain a better hold on the actual spatial variation.

The temperature was controlled to within ± 1 mK and experiments were conducted both by heating and cooling the mixture. The critical point was determined to be $T_c = 336.551$ K. However, drifts in T_c of order 1 mK were observed and comparable gradients may have been present across the sample cell.[6,30]

The correlation length amplitude, ξ_0 [see (1.7)], which is essential to our analysis, can be estimated from turbidity measurements. A supplementary experiment and analysis by Wu[30] yielded

$$\xi_0 = 1.8 \pm 0.7 \text{ Å} . \tag{2.1}$$

The uncertainty, though undesirably large, does not play a significant role in our study of the data; it amounts, in effect, to a translation of the logarithmic temperature scale which is small relative to the full region explored. The reflectivity seems fairly insensitive to a change in ξ_0. Purely for convenience, we have adopted $\xi_0 = 2.0$ Å.

In calculating the dielectric constant profile from the scaled profile according to (1.18), the values

$$\epsilon_\beta(T = T_c) = 1.8526 \quad \text{and} \quad \epsilon_\gamma = 2.2955, \tag{2.2}$$

were adopted.[31] For the scale factor ϵ_0, which, as mentioned, can for most purposes be absorbed into the value of $\tilde{m}_0$, we adopted the SWF value $\epsilon_0 = 0.77$. The determination of the bulk dielectric constant $\epsilon_\infty(T)$ is a more subtle and important issue which we discuss in some detail in Sec. II C.

B. Reliability of the Born approximation

As discussed in Sec. I, the reflectivity may be calculated, for a given dielectric profile, by integrating Maxwell's equations numerically, following the theory developed by Born and Wolf.[32] Alternatively, the reflectivity may be calculated using the Born approximation, which results if one neglects the effect of the profile on the incoming wave. The reflectivity is then simply proportional to the Fourier transform of the dielectric profile which is, of course, linear in the composition profile $m(z)$. However, the use of a cutoff ϵ_β in the dielectric profile in (1.18) destroys a fully linear relation between the reflectivity and the scaled profile, even within the Born approximation. Note that if the reflectivity were completely linear in $m(z)$, the calculation of $\tilde{m}_0(t)$ from the reflectivity data would then involve merely division or normalization. Since this condition does not hold, even within the Born approximation with a cutoff, an iterative procedure for finding $\tilde{m}_0(t)$ was always adopted. We used the Van Wijngaarden–Dekker–Brent method of rootfinding.[33] The calculations are sufficiently compact that little computation time is spent on iteration.

Test calculations by Franck[34] for the pure exponential profile, (b) in Sec. I D, showed that the Born approximation results could deviate by up to 30% from the results of the more precise optical theory based on the integration of Maxwell's equations.[32] Note that if the deviation between the two results were by a constant or slowly varying factor it would not seriously affect an analysis of the profile shape (and its approximate magnitude). On the other hand, we have found, we have found, by explicit calculation, that the temperature dependence of the effective amplitude function $\tilde{m}_0(t)$ for the Born approximation differs significantly from the results of the precise theory for all of the model profiles studied. This is evident from Fig. 3, where we have plotted $\tilde{m}_0(t)$ for the hyperbolic sine profile (d) in Sec. I D, using both methods. The full optical theory yields an appreciably smaller variation in $\tilde{m}_0$ than the Born approximation: this is an encouraging feature in principle, but is subject to caution since other factors also affect $\tilde{m}_0(t)$. However, all the other profiles show similarly qualitative changes. Because of the significant differences between the Born approximation and the full theory, the latter was used in all of the fits described below and shown in the figures.

The optical theory of Born and Wolf is readily programmed and quickly executed. If the dielectric constant varies in the z direction, then, according to the optical theory, the electromagnetic fields at $z = z_f$, say, can be obtained from the fields at $z = z_i$ by a linear transformation, represented by a 2×2 matrix. The coefficients of this matrix are solutions of Maxwell's equations, which we obtain by integrating two coupled first-order differential equations numerically. We found the Bulirsch-Stoer method of integration[33] to be both reliable

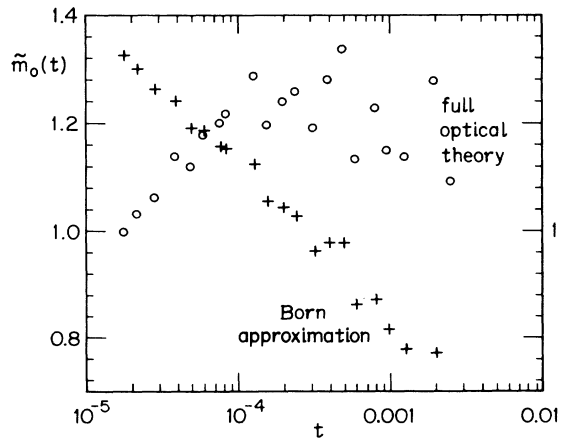

FIG. 3. Plots of $\tilde{m}_0(t)$ for the hyperbolic sine profile (d) with $\nu = 0.631$ and $\beta = \frac{1}{2}\nu$, illustrating the differences between the full optical theory and the Born approximation in matching the reflectivity data of SWF.

and efficient for all the profiles listed in Sec. I D except for the slab profile, which can be solved analytically.[32] Many authors[7,15,26] have used a slightly different approach to calculate the reflectivity (or ellipticity) from Maxwell's equations: the profile is divided into many thin slabs parallel to the interface; the dielectric constant within each slab is approximated by a constant, and the solutions to the differential equations are then obtained by a sequence of 2×2 matrix multiplications, rather than by direct numerical integration. This approach is equivalent to using Euler's method of integration with a fixed integration step size (i.e., the size of the slabs),[33] which leads to uncontrolled errors in the integration. The Bulirsch-Stoer method, on the other hand, computes for various integration step sizes and extrapolates to zero step length. While the numerical differences between the two approaches are probably insignificant for slowly varying profiles, it seems preferable, especially close to the critical point, to use the more accurate Bulirsch-Stoer method, which involves less computational time and no more programming effort that the Euler method.

C. The bulk refractive index

As discussed in Sec. I, the local dielectric constant $\epsilon(z)$, probed in a reflectivity experiment, can be decomposed into a background term ϵ_∞ determined by the refractive index of the bulk fluid, and a piece proportional to the profile function $m(z)$. One may attempt to estimate the bulk, or background contribution to the refractive index by examining the reflectivity data far from T_c; SWF examined the range $1.3\times10^{-3}<t<5.2\times10^{-3}$. In this regime, there should be only a small contribution from the adsorption profile, so the reflectivity should essentially measure the bulk index of refraction. If one assumes first that there is *no* contribution from the profile in this regime, one may calculate the bulk index of refraction $\sqrt{\epsilon_\infty}$ for each reflectivity-temperature data point in this range. Then, as proposed by SWF, one may fit $\sqrt{\epsilon_\infty}$ to the theoretically anticipated form

$$\sqrt{\epsilon_\infty}(t)=\sqrt{\epsilon_c}+Dt+D_\alpha t^{1-\alpha}\ , \tag{2.3}$$

where the specific heat exponent α is reasonably taken as 0.11 (Fisher and Chen[4] conclude $\alpha=0.104\pm0.003$ *via* hyperscaling.) The form (2.3) can then be used to extrapolate $\sqrt{\epsilon_\infty}(T)$ closer to the critical point for use in (1.18).

We refined this initial fit to the background by calculating $\sqrt{\epsilon_\infty}(T)$ iteratively until self-consistency was achieved. A form of the profile must be assumed; for this, it was judged adequate to employ the exponential profile (b) in Sec I D. The initial background fit was used in fitting the profile to the data in the range $10^{-5}<t<10^{-3}$, near T_c. Then, adopting a representative value of $\tilde{m}_0$, we extrapolated the profile to the regime away from T_c used for the initial background fit. On that basis, the background was recalculated, and the process repeated to find a self-consistent estimate of $\sqrt{\epsilon_\infty}$. In fact, the effects of this refinement were found to be small: the coefficient $\tilde{m}_0(t)$ (for the exponential profile) changes by less than 3% over the entire range $10^{-5}<t<10^{-3}$.

On the other hand, it was found that the extrapolation close to the critical point cannot be done with satisfactory accuracy because the last two terms in (2.3) contribute in a significantly different way for $t<10^{-3}$ or 10^{-4}, but are practically indistinguishable further from T_c, where the background is fitted. To address this issue, three cases of (2.3) were considered: (i) with $D_\alpha\equiv0$, (ii) with $D\equiv0$, and (iii) with both D and D_α as adjustable parameters. All three forms fit the data away from T_c within the experimental noise, as seen in Fig. 4. However, the third form (iii) does provide a closer fit even though one worries that one might only be fitting a fluctuation in the data!

For these three almost equally good fits, it was found that the fitted amplitude $\tilde{m}_0(t)$ was highly sensitive to the background, both as regards the assumed form used for fitting $\sqrt{\epsilon_\infty}$, and as regards the fitted values of the parameters $\sqrt{\epsilon_c}$, D, and D_α. For example, Fig. 5 displays $\tilde{m}_0(t)$ for the power-law–exponential profile (c) in Sec. I D with $c=0.1$, using the three fits (i)–(iii). Not only are the amplitudes significantly different, but the systematic trends with t are quite distinct. [The curves shown in Fig. 5 have been rescaled to ease comparison of the goodness of fit. For this purpose, it is convenient to rescale $\tilde{m}_0(t)$ by an overall factor of $1/m_R$, with $m_R=\tilde{m}_0(t_R)$ so that the reduced value at a reference temperature t_R, usually chosen as 7.94×10^{-4}, is unity.]

The sensitivity to a change in the numerical parameters for a given form is even more disconcerting: in Fig. 6, $\tilde{m}_0(t)$ is plotted for our fit of $\sqrt{\epsilon_\infty}$ to a linear variation, and SWF's independent fit to a straight line, which is slightly different. Explicitly, if we accept $\epsilon_\gamma=2.304$ in place of (2.2) (Ref. 31) we find

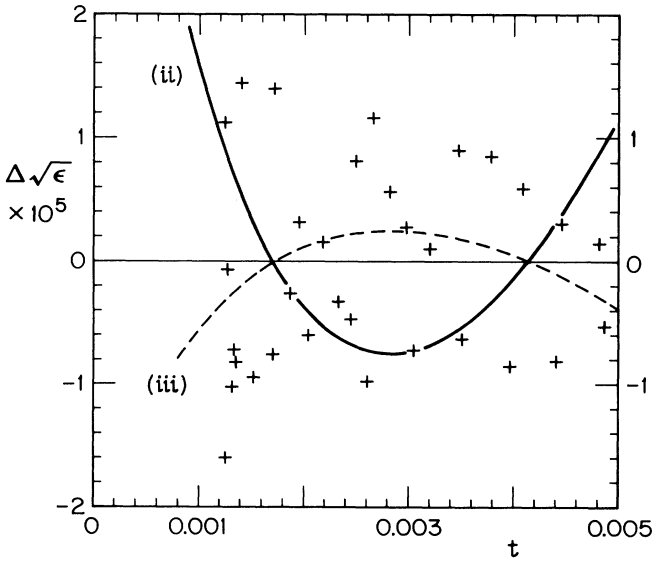

FIG. 4. The deviation of the bulk index of refraction $\sqrt{\epsilon_\infty}$ from a linear fit, $D_\alpha\equiv0$ in (2.3), vs reduced temperature t. The data points derive from the reflectivity-temperature data of SWF. The solid and dashed curves represent the deviations of the fits (ii) with $D\equiv0$, and (iii) with both D_α and D free, from the linear fit. Naturally, (iii) provides the best fit.

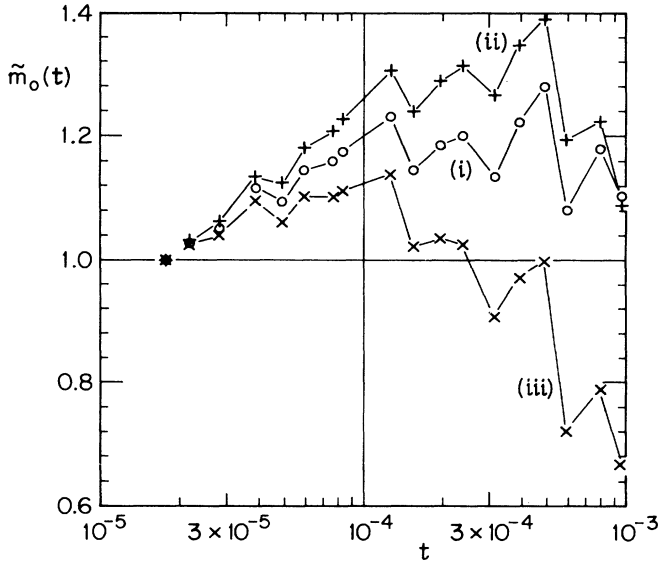

FIG. 5. Plots of $\tilde{m}_0(t)$ (rescaled to unity at $t_R = 1.77\times10^{-5}$) for the power-law–exponential profile (c) with $c = 0.1$, for the three background refractive index fits, (i), (ii), and (iii); see text. The rescaling factors are $m_R = 0.98$, 1.03, and 0.94 for (i)–(iii), respectively. (The Lorentz-Lorenz factor ϵ_0 has been absorbed into $\tilde{m}_0$; see Ref. 22.)

$$\sqrt{\epsilon_c} = 1.483\,96, \quad D = -0.2599 \quad (D_\alpha \equiv 0)\,, \tag{2.4}$$

while SWF quote

$$\sqrt{\epsilon_c} = 1.4841, \quad D = -0.2617 \quad (D_\alpha \equiv 0)\,. \tag{2.5}$$

The difference between these two fits amounts essentially to a constant displacement

$$\Delta\sqrt{\epsilon_\infty} \simeq \Delta\sqrt{\epsilon_c} \simeq 0.000\,14\,.$$

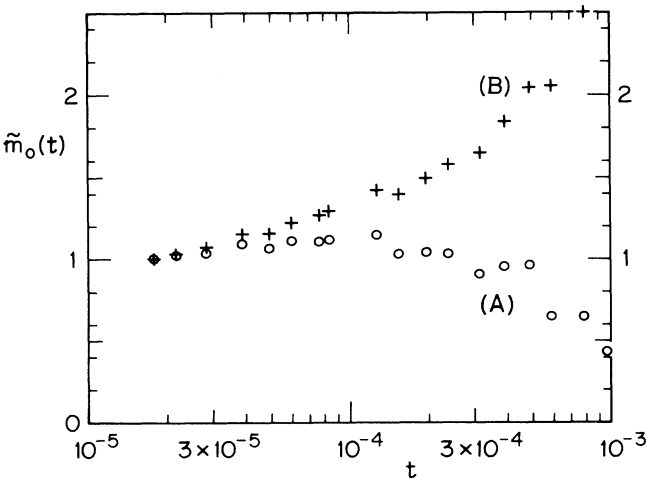

FIG. 6. Plot of $\tilde{m}_0(t)$ (rescaled) calculated from SWF's data for the power-law–exponential profile (c) with $c = 0.1$, for two background refractive index fits: (A) the linear-fit form (2.4) and (B) SWF's linear fit (2.5). (The rescaling factors are $m_R = 0.95$ and 1.07, respectively.)

The origin of this difference is not known; numerically it is very small, but as demonstrated, it makes a significant difference in the analysis. Except for Figs. 5 and 6 where the different backgrounds are compared, all of our fits have used the linear form (i) but with parameters

$$\sqrt{\epsilon_c} = 1.481\,256, \quad D = -0.267\,18 \quad (D_\alpha \equiv 0)\,, \tag{2.6}$$

based on (2.2).[31]

It is evident that it would be valuable to have an independent, direct way of measuring the bulk refractive index through the temperature range $T < 10^{-3}$ which does not rely on fitting outside this regime and extrapolating inwards. Ideally this could be done in the same sample cell as the reflectivity is being measured. Such a procedure was used by Schmidt and Moldover in their ellipsometry experiments.[7,8]

D. Nature of scaling profile

Despite the difficulties in estimating the background, described above, our analysis of the data over nearly two decades, $t = 10^{-5}$ to 10^{-3}, close to T_c, reveals clear evidence of a power-law regime in the profile. To establish this, first consider the simple slab profile, (a) in Sec. I D. In this case, the reflectivity can be calculated analytically.[32] The resulting effective amplitude function $\tilde{m}_0(t)$ is strongly temperature dependent, varying by a factor of roughly 4 over the temperature range of the experiment: see Fig. 7. By contrast, the other profiles listed in Sec. I D yield effective amplitude functions which vary by less than 30% over the same temperature range. We conclude that the data clearly discriminate against the slab profile.

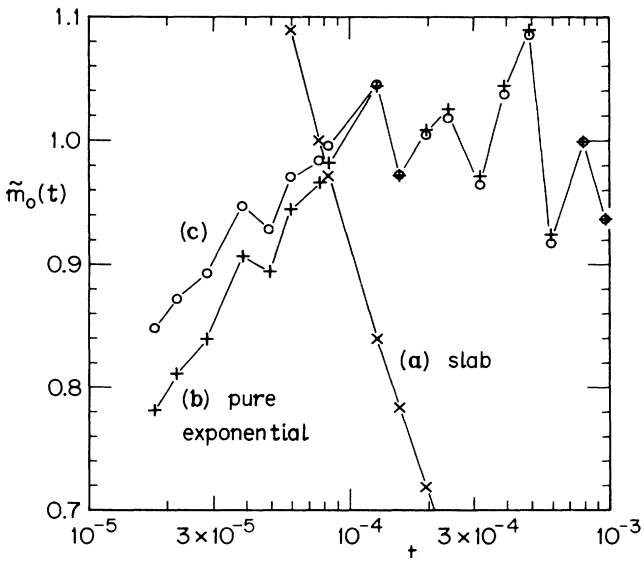

FIG. 7. Analysis of SWF's reflectivity data: rescaled $\tilde{m}_0(t)$ for (a) the slab profile, (b) the pure exponential profile, and (c) the power-law–exponential profile (c) with $c = 0.1$. The fractional variation in $\tilde{m}_0$ is smallest for the power-law–exponential profile. [The rescaling factors are $m_R = 0.097$ for (a) with reference temperature $t_R = 5.94\times10^{-5}$, and $m_R = 1.55$ and 1.15 for (b) and (c), respectively, with $t_R = 7.94\times10^{-4}$.]

Next consider the pure exponential profile (b) in Sec. I D. This can be tested by comparing corresponding fits with fits of (c)–(e), which embody a power-law tail. Figure 7 shows a plot of $\tilde{m}_0(t)$ comparing (b) with the power-law–exponential form (c) with $c=0.1$. Although the influence of the background estimates must be borne in mind, the latter yields an overall variation in $\tilde{m}_0(t)$ which is smaller by a factor of roughly 1.5. Direct plots of the dielectric constant profiles following from (c) with $c=0.1$ are shown in Fig. 2 for various values of t. Note that a fixed value $m_0=1.0$ has been chosen which represents all the data moderately well. See also Fig. 1 for a portrayal of the corresponding scaling function $P(x)$.

By varying c in the form (c) in Sec. I D and by comparing with the sinh profile (d) and the exponential-Padé profile (e), one finds that the goodness of fit is improved if, for a given t, the power-law region extends to larger values of z. In particular, the hyperbolic sine profile (d) resembles a pure exponential too closely and is not favored. However, because of the significant systematic deviations from constancy in $\tilde{m}_0(t)$ observed in all cases (see, e.g., Fig. 7), it is difficult to draw very firm conclusions from the data although we can conclude, for example, that the goodness of fit is better for form (c) with values of c in the range $0.05 \lesssim c < 1$, than for larger values.

By the same token, various scaling functions which exhibit similar crossover from power-law to exponential decay yield comparably good fits. In particular, we find that the forms (c) with $c=0.1$ and (e) with $c=-0.75$ yield nearly identical fits. Thus, in the range $10^{-5} < t < 10^{-3}$, the difference between the effective amplitude functions varies only from 0.098 to 0.12. Such difference are negligible in comparison with the overall deviation from constancy (roughly 20%) for these profiles: see Fig. 7. Although they yield comparable fits, the different scaling functions do differ in form, so one cannot determine much more about the optimal profile beyond the existence of a clear power-law regime. It appears likely, however, on the basis of the reflectivity data, that the universal amplitude ratio P_∞/P_0, controlling the relative strengths of the exponential and power-law pieces, lies in the range 0.2 to 1.0. Furthermore, the optimal profiles all saturate, indicating that for $t \leq 10^{-3}$, a layer of pure nitromethane of thickness $z_0=16$–19 Å is adsorbed on the glass wall, as one anticipates.

Finally, one must consider the effect of uncertainties in the measured critical temperature T_c. If we allow shifts in T_c of a few millikelvin, which may not be outside the actual experimental uncertainties, we find that the systematic downward curvature associated with even the best profiles can be substantially reduced. Indeed, as shown in Fig. 8, an imposed shift of $\Delta T_c=-2$ mK yields an effective amplitude function which is constant within the experimental scatter. Thus, it appears that the systematic deviation from constancy in $\tilde{m}_0$ may stem to some degree from inaccuracies in T_c as well as from imprecision in the determination of the bulk index of refraction. Improvements in both these experimental aspects should be possible in the future, so it is reasonable to hope that more definitive conclusions about the scaling profile can be reached.

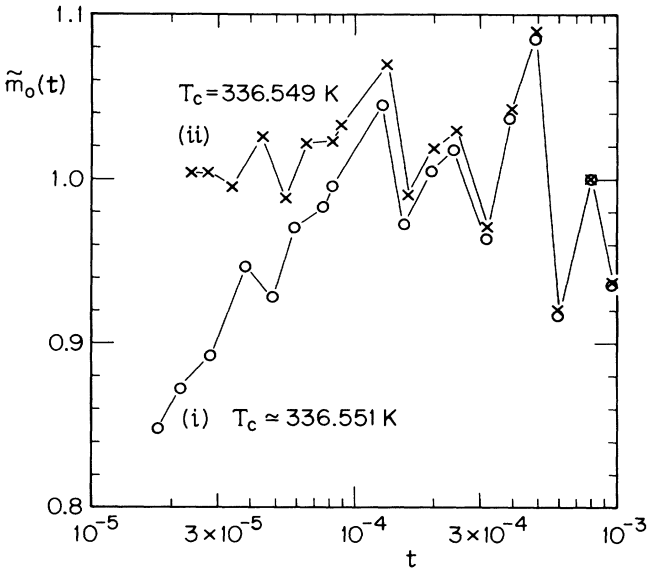

FIG. 8. Plots of the rescaled $\tilde{m}_0(t)$ calculated from SWF's data for the power-law–exponential profile (c) with $c=0.1$, for (i) no T_c shift (open circles), and (ii) a T_c shift of -2 mK (crosses). The second shift is on the borderline of the uncertainties that may be allowed by the experimental observations. [The rescaling factors are $m_R=1.154$ and 1.157 for (a) and (b), respectively, with $t_R=7.94\times10^{-4}$.]

III. ELLIPSOMETRY

A. Experiment

Ellipsometry data taken by Schmidt and Moldover[7] on isopropanol-perfluoromethylcyclohexane (i-P+pFMCH) and by Schmidt[8] on methylcyclohexane-perfluoromethylcyclohexane (MCH+pFMCH) against their vapor-liquid interfaces have been analyzed by a strategy similar to that described above. In both experiments, the mixtures were prepared at several compositions, but the analysis presented here concerns only the samples at critical composition. The sample cell was designed so that light could enter via two optical paths. The index of refraction of each sample was measured along one optical path while, at the same time, the coefficient of ellipticity was measured by reflecting light from the vapor-liquid interface along the other path. The critical temperature was determined from the index of refraction data below the transition, to an accuracy of 10 mK. However, relative changes in T can be observed to a precision of a few millikelvin.

The ellipsometry observations were made using light from a He Ne laser (of wavelength 6328 Å) at the Brewster angle $\theta_1=\theta_B$ which depends on the local dielectric constant of the vapor and liquid, and thus varies with temperature. The ellipsometer was adjusted to the Brewseter angle at each temperature.

Most of the data on the i-P+pFMCH mixture[7] were taken at a steady cooling rate of 0.03 K/h or slower.

Schmidt's data on the MCH+pFMCH mixture, on the other hand, were taken at equilibrium,[8] which is clearly preferable since noticeable hysteresis was observed in the first system. The sample was equilibrated for 10 to 12 h at each temperature and around 30 measurements were then taken over a half-hour period. The data points shown in the figures below represent averages of these repeated observations.

The correlation length amplitude ξ_0 [see (1.7)] was estimated from measurements of the surface tension amplitude σ_0. According to hyperuniversality, ξ_0 and σ_0 form a universal ratio[35] which has been estimated on the basis of experiments[36] to be

$$\sigma_0(\xi_0)^2/k_B T_c \simeq 0.386 \ . \tag{3.1}$$

For the i-P+pFMCH mixture, Schmidt and Moldover obtained σ_0 from measurements of the density difference and the capillary length,[7,37] and *via* (3.1) then concluded

$$\xi_0 \simeq 1.9 \text{ Å} \ . \tag{3.2}$$

Recently, the capillary rise data were reanalyzed by Schmidt,[8] who concluded that a more reliable estimate would be $\xi_0 \simeq 2.6$ Å. For the MCH+pFMCH mixture, similar experiments[38] yielded an estimated correlation length amplitude of

$$\xi_0 \simeq 2.79 \text{ Å} \ . \tag{3.3}$$

The uncertainties in (3.2) and (3.3) are difficult to assess. The universal ratio (3.1) is remarkably difficult to ascertain with precision; experimental estimates range from 0.3 to 0.5, implying an uncertainty of at least 25% in (3.1).[36] The surface tension amplitude estimates are also subject to significant uncertainty. Unfortunately, our analysis of the ellipticity data proves to be fairly sensitive to the value of ξ_0, as demonstrated in Sec. III C below.

In calculating the dielectric constant profile, we accepted the values

$$\epsilon_\beta(T_c)=1.558 \quad \text{and} \quad \epsilon_\infty(T_c)=1.6440 \ ,$$

$$T_c = 361.992 \text{ K} \tag{3.4}$$

for the i-P+pFMCH mixture and

$$\epsilon_\beta(T_c)=1.608 \quad \text{and} \quad \epsilon_\infty(T_c)=1.7766 \ ,$$

$$T_c = 318.29_0 \text{ K} \tag{3.5}$$

for the MCH+pFMCH mixture, as given by Schmidt and Moldover.[7,8] Recently, Schmidt has revised the estimates of the critical temperatures for these samples; see Ref. 8 for more details. In both cases, we take $\epsilon_\gamma = 1.000\,0$ for the vapor phase.

We also need to know the correlation length ξ_γ in the vapor phase. For i-P+pFMCH, Schmidt and Moldover studied ellipticity data at the liquid-vapor interface of pure pFMCH and of the mixture well above T_c. By fitting to an assumed tanh profile (see below) they concluded that

$$\xi_\gamma \simeq 6 \text{ Å} \tag{3.6}$$

described both situations. Schmidt subsequently discovered that the value quoted above is incorrect by a factor of 2.[8] He has since recalculated ξ_γ for the two pure fluids using the Fisk-Widom profile, and concludes that a better estimate would be $\xi_\gamma \simeq 3.3$ Å.[8] This revision does not affect our analysis, for reasons explained in Sec. III C. For MCH+pFMCH, Schmidt[8] obtained vapor-liquid ellipticity data for pure MCH and for pure pFMCH. We have fitted these data both with the tanh profile and with the Fisk-Widom profile (see below). This led to values in the range

$$\xi_\gamma \simeq 1.6\text{–}2.4 \text{ Å} \tag{3.7}$$

for both components over a range of temperatures. For the present analysis, it suffices, in view of other uncertainties (see below), to adopt $\xi_\gamma = 2.0$ Å.

B. Model profiles

The overall strategy used to analyze the ellipsometry data for critical adsorption is the same as for the reflectivity data. In particular, trial profiles are assumed to be known, apart from an amplitude factor m_0. The model profiles used for the ellipsometry experiments must, however, be more complicated because the adsorption occurs against the vapor-liquid interface, rather than against a glass substrate. It is no longer reasonable to model the $\gamma\beta$ interface by a sharp cutoff, as in Fig. 1. Instead, model profiles for the vapor side of the interface should be matched on to the scaled adsorption profiles (a)–(e) listed in Sec. I D.

As before, we work directly with the dielectric constant rather than the composition. (Within the liquid phases we may assume the validity of the Lorentz-Lorenz relation,[22] but we again absorb the scale factor, ϵ_0 into the value of $\tilde{m}_0$.) Consider the dielectric profile of the vapor-liquid interface when the critical adsorption is neglected: we will suppose it can be written as

$$\epsilon_{vl}(z)=\tfrac{1}{2}(\epsilon_\lambda+\epsilon_\gamma) + \tfrac{1}{2}(\epsilon_\lambda-\epsilon_\gamma)\tilde{P}[(z-z_0)/\xi_\gamma] \ , \tag{3.8}$$

where ϵ_λ is a *nominal* value for the dielectric constant of the liquid, ϵ_γ is the dielectric constant of the vapor, z_0 specifies the location of the interface, and ξ_γ is the correlation length in the vapor. We have considered four models for the function $\tilde{P}(x)$, which specifies the nature of the (noncritical) vapor-liquid interface profile. The first is a simple step analogous to the model used in Sec. II and depicted in Fig. 2, where the glass was treated as structureless; specifically, we take the following.

(w) *Sharp interface form:*

$$\tilde{P}(x)=\pm 1 \quad \text{for } x \gtrless 0 \ , \tag{3.9}$$

with $\epsilon_\lambda=\epsilon_\beta$ and $z_0=0$. Note that other forms of sharp profile might well be considered. More realistic is the following form predicted by mean-field theory.

(x) *Tanh form:*

$$\tilde{P}(x)=\tanh\tfrac{1}{2}x \ . \tag{3.10}$$

As an improvement over this, Fisk and Widom[27] proposed the following form.

(y) *Fisk-Widom form:*

$$\tilde{P}(x)=\frac{\sqrt{2}\tanh\frac{1}{2}x}{(3-\tanh^2\frac{1}{2}x)^{1/2}} \ , \tag{3.11}$$

on phenomenological grounds primarily applicable in the

critical region (which, of course, is not actually the situation here). Finally, for use purely on the vapor side of the interface, we consider the following form.

(z) *Exponential tail form:*

$$\tilde{P}(x) = -1 + e^{-|x|}/(1-e^{-|x|}) \quad \text{for } x < 0 \, . \tag{3.12}$$

This diverges as $x \to 0^-$, which is unphysical; however, when this profile is matched to the critical adsorption profiles (a)–(e) of Sec. I D, the matching points satisfy $x^* < 0$, so that the overall profile is well behaved.

The aim now is to match the vapor-liquid interfacial profiles to the critical adsorption profiles in order to obtain an overall model profile $\epsilon(z)$. For the critical adsorption profile we adopt

$$\epsilon_{\alpha\beta}(z) = \epsilon_\infty - \epsilon_0 m_0 t^\beta P(z/\xi_{\alpha\beta}) \, , \tag{3.13}$$

[as before; see (1.18) and (1.3)] where ϵ_∞ is the bulk dielectric constant of the binary fluid mixture. Several matching schemes were tried; not all prove successful for the various critical adsorption profiles. Three methods found most useful are specified by the following.

(i) *Exponential match.* To match the exponential adsorption profile (b) in Sec. I D to the vapor-liquid profiles (x) or (y) we treat ϵ_λ and z_0 in (3.8) as parameters and match (3.13) smoothly, in value and slope, at $z = 0$.

(ii) *Strong power-law–exponential match.* This method is applicable with the adsorption profiles (c)–(e) in Sec. I D when m_0 is not too small. The nominal liquid value ϵ_λ in (3.8) is equated to ϵ_β, as in (w), which is physically reasonable when the adsorption layer is sufficiently thick that it resembles pure liquid B. Then (3.8) and (3.13) are smoothly matched, in value and in slope, to (x), (y) or (z) at some point $z = z^*$ found by adjusting z_0.

(iii) *Weak power-law–exponential match.* If, in using the profiles (c)–(e) in Sec. I D, the amplitude m_0 is too small to yield a solution in (ii), we set ϵ_λ equal to ϵ_∞ (in place of ϵ_β). This is plausible when the adsorbed layer is thin, since the liquid near the interface resembles the bulk liquid mixture more closely than the pure phase B. Then z_0 is adjusted, as in (ii), to achieve a smooth join at some point $z = z^*$.

A comparison of the vapor profiles (w)–(z) when matched onto the same power-law–exponential liquid profile (c) in Sec. I D is shown in Fig. 9. As might be expected, the results do not differ drastically in numerical terms.

C. Dependence of ellipticity on the profile parameters

Our primary aim, of course, is to determine the degree to which the various scaled critical adsorption profiles (a)–(e) in Sec. I D can represent the ellipticity data. Because of the complications resulting from the presence of vapor, however, we proceed, first, to study the changes in the ellipticity versus temperature plots produced by systematically varying some of the ancillary parameters we have been led to introduce. In particular, we need to understand the degree to which the choice of profile, (w)–(z) in Sec. III B, for the vapor side of the interface affects the calculated ellipticity $\bar{\rho}_B(T)$. According, we have assumed various plausible adsorption profiles, held them fixed, and computed $\bar{\rho}_B(T)$ for the profiles (w)–(z). Part A of Fig. 10 shows the results obtained for the power law–exponential profile (c) in Sec. I D with $c = 0.7$ when combined using the matching procedure (iii) with the four vapor-side profiles (w)–(z) in Sec. III B. The overall

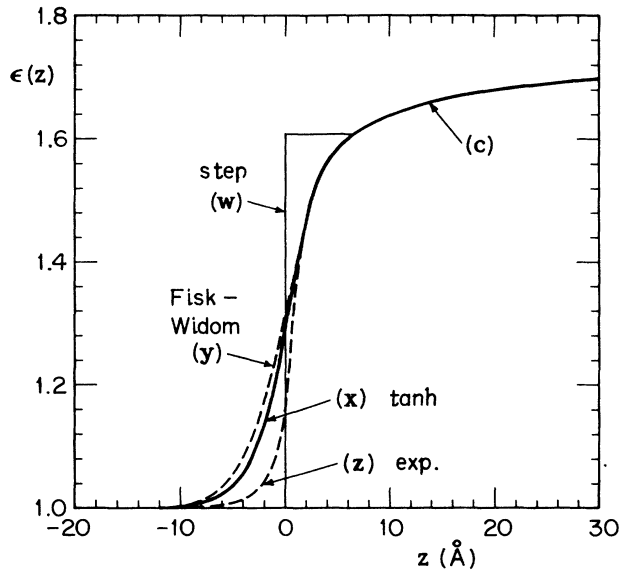

FIG. 9. Model dielectric constant profiles for the vapor-liquid mixture interface illustrating the matching of four vapor-side profiles (w)–(z) [see Eqs. (3.8)–(3.11)] onto a fixed critical adsorption profile, namely, the power-law–exponential scaled form (c) with $c = 0.7$, $m_0 = 0.29$, $\xi_0 = 2.79$ Å and $t = 10^{-4}$. Note that the scaled profile alone would diverge negatively at $z = 0$.

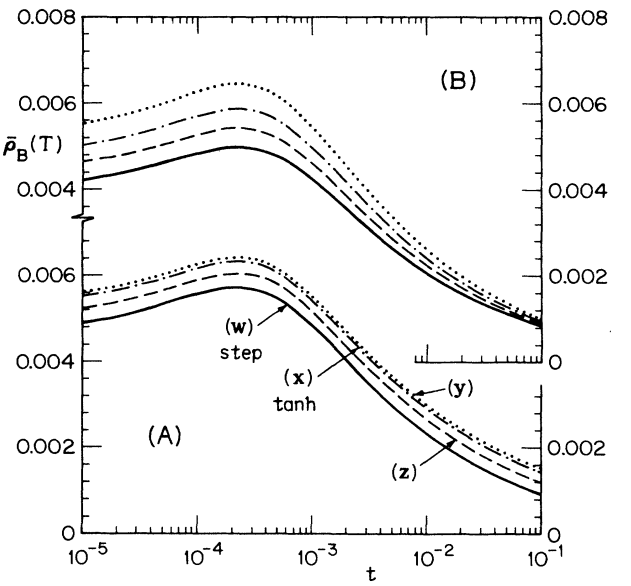

FIG. 10. (A) Calculated ellipticity coefficients for the four overall vapor-liquid profiles illustrated in Fig. 9. The different vapor-side profiles evidently lead to distinct but essentially temperature-independent vertical shifts. (B) Ellipticity coefficients calculated using the step profile (w) for the vapor side of the interface and the critical adsorption profile (c) with $c = 0.7$ and $\xi_0 = 2.79$ Å for the sequence of amplitudes $m_0 = 0.25$ (solid curve), 0.27, 0.29, and 0.32 (dotted curve).

profiles are just those illustrated in Fig. 9. Evidently, the choice of vapor profile has a marked effect on the values of $\bar{\rho}_B(T)$, amounting to about 10% of the maximum value of $\bar{\rho}_B$ (which occurs here, as in the real data, around $t = 10^{-3}-10^{-4}$), but to 50% or more of the lower values (found near $t \simeq 10^{-1}$). Fortunately, however, the differences between the various vapor profiles are almost exactly representable by *temperature-independent* shifts in $\bar{\rho}_B$. This is physically reasonable since the vapor-liquid interface is far from criticality so that the vapor side of the profile should change very little over the temperature range of interest ($t \lesssim 0.1$). However, since we cannot really distinguish on theoretical grounds between the profiles (x), (y), and (z) or other reasonable choices, even if we agree to rule out (w), we must recognize that *in essence* the ellipticity data are, as regards determination of the critical adsorption contribution, uncertain up to an additive constant, say $\Delta\bar{\rho}$, of magnitude possibly as large as 0.001. (We find that other matching procedures lead to similar shifts.)

Consider, next, the correlation length amplitude ξ_0 which, as explained, is subject to significant numerical uncertainties. Changing the assignment of ξ_0 should be roughly equivalent to multiplying the reduced temperature by a constant factor, provided one allows for a complementary change in the value of the amplitude m_0. Thus on a plot of $\bar{\rho}_B(T)$ versus log$t$, a variation in ξ_0 should mainly give rise to a horizontal translation of the graph. This surmise is confirmed by explicit test calculations. Thus we must, in effect, also regard the data plots of $\bar{\rho}_B$ versus log$t$ as subject to shifts parallel to the temperature axis of up to, perhaps, a fifth or so of a decade.

Finally, we inquire into the nature of the changes induced in $\bar{\rho}_B(T)$ by altering the amplitude m_0. Because the critical adsorption profile changes dramatically as $\xi(T)$ varies, this cannot amount to a temperature-independent shift. Rather, as illustrated in part (B) of Fig. 10, one finds that for temperatures below the maximum in $\bar{\rho}_B$, i.e., for $t < t_{\max} \simeq 3\times 10^{-4}$, the differences in $\bar{\rho}_B$ are proportional to the changes in m_0, while for higher temperatures this linearity is rapidly lost. Physically, one understands the fact that $\bar{\rho}_B$ increases more slowly than m_0 for $t > t_{\max}$ by noting that as t increases the critical adsorption profile weakens and contributes progressively less to the ellipticity relative to the steep, unchanging vapor side of the overall profile. Indeed, far above T_c the ellipticity approaches a constant, controlled by the vapor-liquid profile, which is independent of m_0. The plots in Fig. 10(B) have been calculated using, again, profile (c) in Sec. I D with $c = 0.7$ and the sharp-step vapor-side profile (w) in Sec. III B. Quite similar results follow when matching to profiles (x), (y), or (z) of Sec. III B.

One concludes that in fitting calculated $\bar{\rho}_B$ versus log$t$ plots to the experimental data one can compensate for changes in m_0 *below* $t_{\max}$ by vertical shifts, corresponding to modifying the vapor-side profiles, whereas *above* $t_{\max}$, varying m_0 changes the slope and, thus, the overall shape of the plots. The location of $t_{\max}$ can be varied, for a fixed critical adsorption profile, by horizontal shifts corresponding to changes in the value of ξ_0. Using these insights into the nature of the fitting problem, we turn now to studying the degree to which the data can be used to discriminate between the different critical adsorption profiles.

D. Optimal scaling profiles

We will analyze first the data of Schmidt[8] for MCH+pFMCH which, as mentioned, were taken under equilibrium conditions. We inquire initially whether the experiment can discriminate clearly against the slab and pure exponential scaled profiles (a) and (b) in Sec. I D. In fact, as shown by the solid curve in Fig. 11, the slab profile with $m_0 = 0.35$ provides a fairly good fit to the data further from T_c, specifically for $t \gtrsim 5\times 10^{-4}$. The plot in Fig. 11 has been computed with the sharp profile (w) in Sec. III B and then shifted upwards by $\Delta\bar{\rho} = 5\times 10^{-4}$ to achieve the fit. This shift is well within the expected range discussed in the previous section. Closer to T_c the ellipticity predicted by the slab profile decreases sharply, and changes sign at $t \simeq 7\times 10^{-5}$. Indeed, the slab model predicts an infinite number of sign changes in $\bar{\rho}_B$ as $t \to 0$. No such behavior is seen experimentally and, clearly, the data for $t \lesssim 5\times 10^{-4}$ discriminate strongly against the slab profile (a).

The pure exponential profile (b) in Sec. I D was tested using matching procedure (i) and vapor-liquid interfacial profiles (w)–(z) in Sec. III B. If the value of $m_0 = 0.6$ is adopted, the exponential profile fits the data fairly well for $t \gtrsim 9\times 10^{-4}$, but decreases too sharply, although not as sharply as the slab profile, for smaller t. The fit for the exponential profile (b) shown by the dashed curve in Fig. 11 is for a match to the sharp vapor-liquid profile (w); no

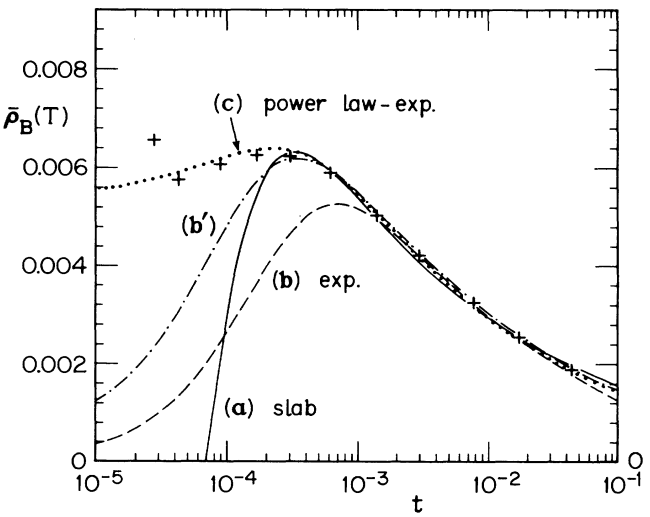

FIG. 11. Various fits to the critical adsorption ellipticity data of Schmidt (Ref. 8) for the MCH+pFMCH mixture: (a) slab profile (solid curve); (b) pure exponential profile with sharp vapor-side profile (w) (dashed curve); (b') exponential profile with shifts (dot-dash curve), (c) power-law–exponential profile (c) with $c = 0.7$ matched to the tanh profile (x) (dotted curve). See the text for further quantitative details.

further vertical shift proves helpful. Note that the exponential profile actually fits well over a *smaller* temperature range than does the slab profile. However, the range of the fit can be extended down to $t \gtrsim 3\times10^{-4}$, as shown by the dot-dashed curve (b′) in Fig. 11, by adjusting the correlation length amplitude from $\xi_0=2.79$ Å to $\xi_0\simeq 1.8$ Å (thus shifting the plot horizontally, as explained above). The required 35% change in ξ_0 implies a 70% change in the amplitude ratio (3.1), but this is larger than seems reasonable, even considering the large uncertainties discussed previously. A vertical shift of $\Delta\bar{\rho}_B=5\times10^{-4}$ and the value $m_0=0.65$ were used for the (b′) plot shown in Fig. 11.

Now consider the power-law–exponential profile (c) in Sec. I D. As discussed in Sec. III B, two different matching procedures (ii) and (iii), are applicable. If the assigned amplitude m_0 is too small, the matching equations used in (ii) have no solution. We find that the minimum value of m_0 for which a solution exists ($m_0\simeq0.41$) yields ellipticities spanning the range $0.0036\lesssim\bar{\rho}_B\lesssim0.009$ over the interval $10^{-5}\lesssim t\lesssim10^{-2}$, the experimental data vary only from 0.003 to 0.006 over the same interval. While the agreement is reasonable near $t\simeq10^{-2}$, the calculated value rise to a maximum which is roughly 50% higher than found in the data. As is to be expected, increasing m_0 only serves to exacerbate this disagreement. To decrease m_0 and still obtain a satisfactory overall model profile, we adopted procedure (iii). Then, the value $m_0\simeq0.29$ yields the optimal fit, allowing for a vertical shift as before. The size of the power-law region can be studied by varying the parameter c. We find that the best fits are provided by $0.6\lesssim c\lesssim0.8$, which correspond to values of the universal ratio P_∞/P_0 of roughly 0.8 to 0.9.

We also find that a match to the tanh vapor-side profile, (z) in Sec. III B, provides the best vertical shift. The resulting fit, shown by the dotted curve in Fig. 11, was computed with $c=0.7$. Note that the data point closest to T_c lies anomalously high. We presume that this represents an experimental artifact which may be neglected in fitting; however, no very cogent reasons can be adduced for this conclusion.

The power-law–exponential profile clearly constitutes a great improvement over the slab and pure exponential profiles. However, an even better fit can be obtained by allowing for changes in T_c. Figure 12(A) depicts a fit obtained with a value of T_c increased by $\Delta T_c=3$ mK above the value quoted in (3.5). The upper part of the figure contains the corresponding effective amplitude plot $\tilde{m}_0(t)$, and, in addition, plots appropriate to $\Delta T_c=0$ and $\Delta T_c=5$ mK. The shift of 3 mK is within the expected experimental uncertainty and provides the best fit, as is evident from the degree of constancy of $\tilde{m}_0(t)$ over two decades, from $t\simeq10^{-3}$ to $t\simeq10^{-5}$ (barring the anomalous point closest to T_c). Indeed, Schmidt's recently revised estimate[8] of T_c, which is higher by 5 mK, agrees well with the results of our analysis. For larger values of t, $\tilde{m}_0$ begins to increase, but the overall variation in $\tilde{m}_0(t)$ over the range $10^{-5}<t<0.1$ is only 7%, and, as mentioned, the data for $t\gtrsim10^{-2}$ are less sensitive to the critical adsorption profile.

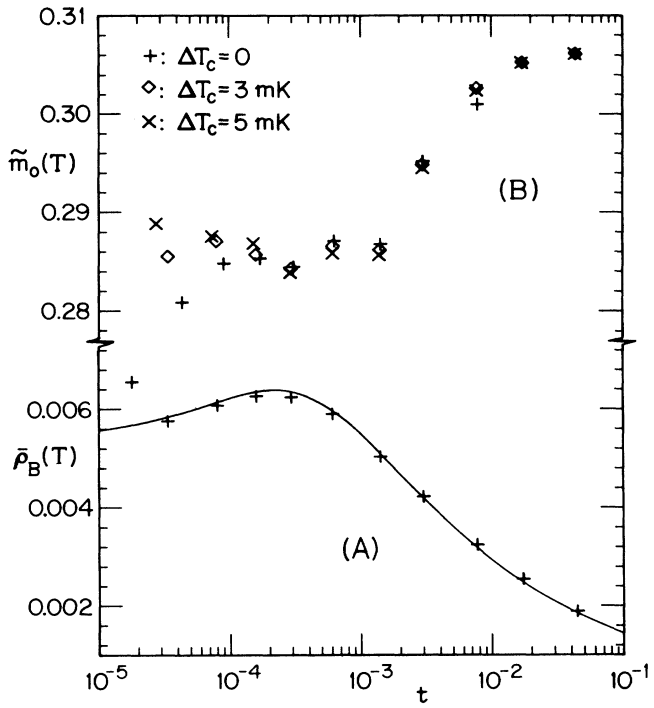

FIG. 12. (A) Fit of the data for MCH+pFMCH to the adsorption profile (c) with $c=0.7$ and a critical point shift $\Delta T_c=3$ mK above the quoted value $T_c=318.290$ K; (B) plots of the amplitude function $\tilde{m}_0(t)$ for fits to the same profile but with T_c shifts of 0, 3 mK, and 5 mK; see the text for discussion.

To test whether the data could distinguish between different profiles which all display crossover from power-law to exponential decay, we also examined the hyperbolic sine (d) and exponential-Padé (e) profiles in Sec. I D. The results are shown in Fig. 13. The hyperbolic sine profile matched to the tanh vapor-side profile (x) in Sec. III B with procedure (iii), with $m_0=0.25$, provides an excellent fit for $t\gtrsim4\times10^{-4}$, but yields ellipticities that are definitely too low at smaller t. A 14% decrease in ξ_0 was employed for this fit.

The exponential–Padé profile provides a nearly satisfactory fit over the entire temperature range, as seen in

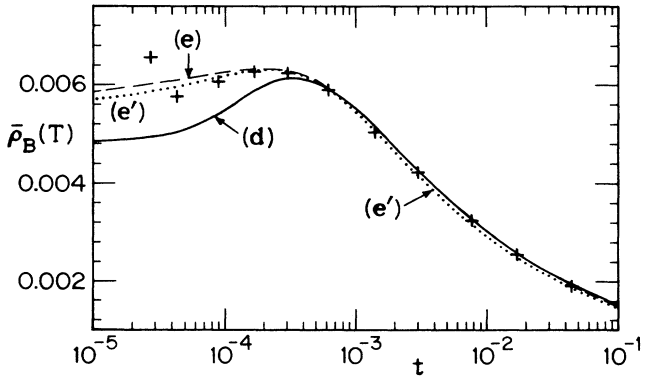

FIG. 13. Fit of the data for MCH+pFMCH to the critical adsorption profiles (d) (solid); (e) with $c=-0.15$ and $\xi_0=3.3$ Å (dashed); and (e′) with $c=0.25$ and $\xi_0=2.79$ Å (dotted): see the text for discussion.

Figs. 13(e) and 13(e'). A characteristic feature of this profile is the very gradual slope in $\bar{\rho}_B$ as t decreases below t_{max} relative to the slope of $\bar{\rho}_B$ above the maximum. This feature appears to be only weakly dependent on the value of the parameter c. In contrast, the other profiles 13(a)–13(d) (and the data), decrease more sharply, like the solid line in Fig. 13. It transpires that the exponential–Padé profile provides a reasonable fit over a wide range of the parameter c. If ξ_0 is fixed at its estimated value, 2.79 Å, the choice $c=0.25$ provides a good fit: see (e') in Fig. 13. [In this fit, profile (e) was matched to the tanh profile (x) using procedure (iii), with $m_0=0.275$.] However, the choices $c=-0.15$, $\xi_0=3.3$ Å [shown in Fig. 13 for (e) matched to (x) with procedure (iii) and $m_0=0.26$] and values of c and ξ_0 between these also prove satisfactory. Hence we can conclude only that the exponential–Padé profile predicts values of the universal ratio P_∞/P_0 in the range 0.9–1.1. The power-law–exponential profile predicts $P_\infty/P_0=0.85\pm0.07$, which is quite consistent with the lower range. Because the former profile provides a better overall fit to the data and yields a smaller uncertainty in P_∞/P_0, we place somewhat more confidence in its predictions. Nevertheless, as explained, the exponential–Padé profile is more satisfactory theoretically and a larger value of P_∞/P_0 would deviate less from the plausible monoticity with dimensionality discussed at the end of Sec. I E.

Finally, we may compare our predictions for the Brewster angle $\theta_B(T)$ to those actually measured in the experiment. As mentioned in Sec. III A, the ellipsometer was automatically adjusted to θ_B at each temperature. In our approach, we first calculate θ_B by setting $\mathrm{Re}(r_p/r_s)=0$ (for a given profile), and then calculate $\bar{\rho}_B=\mathrm{Im}(r_p/r_s)$. Thus, a comparison of theoretical and experimental results for $\theta_B(T)$ provides an independent check of our analysis. The Brewster angles were measured by Schmidt[8] for the MCH+pFMCH mixture with an experimental precision within 0.01° but were accurate only up to a uniform uncertainty of 0.3° or more. Figure 14 displays a comparison of $\theta_B(T)$ calculated from fits to $\bar{\rho}_B(T)$ for our various model profiles, with the observed data. The experimental values have all been shifted by 1.05×10^{-3} radians, or 0.06°, but this is well within the anticipated experimental accuracy limits. The power-law–exponential and exponential–Padé profiles, (c) and (e) in Sec. I D, provide the best agreement, as they do for the coefficient of ellipticity. The close agreement between the predicted and measured Brewster angles is an encouraging confirmation of the reliability of our analysis.

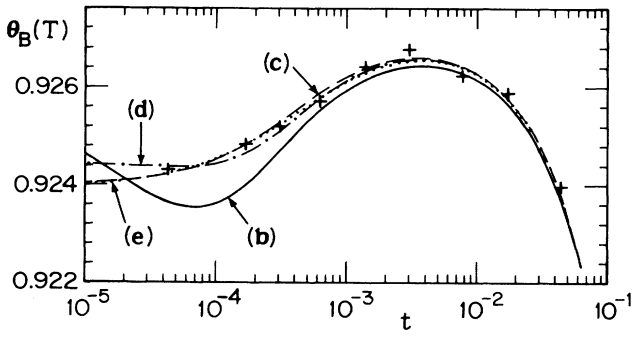

FIG. 14. Plots of the Brewster angle $\theta_B(T)$ from Schmidt's experiment and as calculated from the fits shown in Figs. 11–13 for adsorption profiles (b)–(e). The power-law–exponential (c) and exponential-Padé (e) profiles provide the best agreement with the data: see the text.

Consider, now, the data of Schmidt and Moldover[7] on i-P+pFMCH displayed in Fig. 15. As in the case of the MCH+pFMCH mixture, the slab and pure exponential critical adsorption profiles unambiguously fail to provide adequate fits close to critical temperature. However, the power-law–exponential profile also proves less than satisfactory. The ellipticity calculated for the profile (c) in Sec. I D with $c=0.7$ and $m_0=0.33$ is represented by the solid curve in Fig. 15. The fit is good for $t\gtrsim5\times10^{-4}$ but the calculated value is too large by roughly 5×10^{-4} below that temperature. (A vertical shift of $\Delta\bar{\rho}=0.0016$ was employed here. We remark, however, that for the parameters best approximating the i-P+pFMCH mixture, the differences entailed in using vapor profiles (w)–(z) in Sec. III B are numerically greater than for the MCH+pFMCH mixture although qualitatively quite similar. Specifically, we may regard the ellipticity data as uncertain up to an additive constant of $|\Delta\bar{\rho}|\lesssim0.002$.)

One possible reason for the fitting discrepancy near T_c is that the system may not have been sufficiently close to equilibrium; this issue will be discussed further in Sec. IV. However, the situation can be improved if $\xi_0=2.7$ Å is used instead of (3.2) and if the critical temperature is shifted by $\Delta T_c=-10$ mK: the diamonds and the dashed curve in Fig. 15 show such a fit using the power-law–exponential profile with $c=0.7$ and $m_0=0.28$, matched to (z) in Sec. III B with procedure (iii). As mentioned in Sec. III A after Eq. (3.2), a recent reanalysis of the capillary rise data has led Schmidt[8] to conclude that a better estimate of ξ_0 would be 2.6 Å rather than 1.9 Å. The new estimate is in excellent accord with our conclusion that $\xi_0\simeq2.7$ Å would yield a better fit. However,

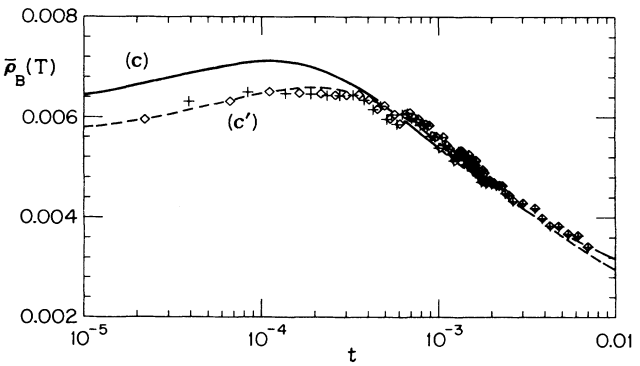

FIG. 15. Fits to the ellipticity observations of Schmidt and Moldover (Ref. 7) on i-P+pFMCH. Crosses represent the data plotted with the reported $T_c=361.992$ K; correspondingly, the solid curve depicts a fit of profile (c) with $c=0.7$. The diamonds represent the data with a shift of $\Delta T_c=-10$ mK, while the dashed curve, labeled (c'), represents the same scaled profile but with the T_c shift and a change in ξ_0: see the text.

the critical temperature shift used here is larger than the experimental uncertainties reasonably allow. Despite this, it is reassuring that both the i-P+pFMCH data and the MCH+pFMCH data prefer the same value of the free parameter, namely, $c=0.7$: this suggests that the ellipticity data are providing significant information about the universal scaled critical adsorption profile beyond the undoubted presence of a strong power-law contribution; in particular, as discussed above, one may conclude, tentatively, that $P_\infty/P_0 \simeq 0.85 \pm 0.20$.

IV. EVALUATION OF REFLECTIVITY AND ELLIPSOMETRY

A. Remarks and suggestions for future experiments

We have shown in Secs. II D and III C that several aspects of the scaled critical adsorption profile $P(x)$ in (1.3), such as the crossover region and the universal ratio P_∞/P_0, can be deduced with appreciably more confidence from the ellipticity data[7,8] than from the reflectivity data.[6] The reason lies partly in the intrinsic strengths and limitations of the two techniques. Ellipsometry is the more sensitive method. If l measures the thickness of the adsorbed layer and λ is the wavelength of incident light, then[26] $\bar{\rho}_B$ is of order l/λ while the reflectivity increment due to the adsorption profile ΔR is of order $(l/\lambda)^2$. Similarly, if $\delta\epsilon$ represents the deviation from a sharp step of magnitude $\Delta\epsilon$, then $\bar{\rho}_B$ is of order $\delta\epsilon/\Delta\epsilon$ and ΔR is of order $(\delta\epsilon/\Delta\epsilon)^2$. Another important advantage of ellipsometry over reflectivity was mentioned in Sec. I; the measured reflectivity depends strongly on a "background" piece R_b with attendant uncertainties. This contribution arises from the dielectric mismatch $\epsilon_\gamma - \epsilon_\infty$ between the substrate and the bulk fluid. (Strictly speaking, the contributions to R from the background and the critical adsorption profile are not additive; this further complicates the problem of unraveling the adsorption profile.) Ellipsometry, on the other hand, is not handicapped by the presence of a background of this sort.

Although these considerations indicate that ellipsometry is the superior technique, it possesses a significant drawback: in a sense it is *too* sensitive. Thus, the calculations described in Sec. III C demonstrate that $\bar{\rho}_B$ is particularly sensitive to the details of the vapor-side profile. This feature is undesirable for our purposes, since the shape of this aspect of the profile is not known and cannot really be determined in an independent manner. On the other hand, the reflectivity is far less sensitive to the substrate details. One should therefore regard ellipsometry and reflectivity as complementary techniques, which, if used appropriately on the same binary mixture against a vapor or solid interface, could together yield substantial reliable information about the scaling profile.

Several improvements need to be made in the experiments, however, before more conclusive results can be obtained. First, and most important in connection with reflectivity, in order to know the background behavior, the bulk index of refraction should be measured as a function of temperature simultaneously with the reflectivity. (This was done by Schmidt and Moldover in their ellipsometry experiments.) Second, as mentioned in Sec. II A, the reflectivity data of SWF were taken at only one incident angle θ_1 very close to the angle of total internal reflection in the glass. At *smaller* incident angles, smaller length scales are probed, so it should be easier to resolve the behavior of the profile in the important region. Test calculations by Xiao-lun Wu[30] for various model profiles indicate that an experiment using smaller angles should be able to resolve reliably the hyperbolic sine profile (d) from the exponential form (b). Optimistically, one might also distinguish among the forms (c), (d), and (e) in Sec. I D. Another advantage to be gained is that each reflectivity-temperature data set for a different angle would share the same background and hence yield further constraints on fitting of the bulk index of refraction. Thus, an approach which *might* prove feasible is to treat the bulk refractive index as a parameter to be adjusted at each fixed temperature T, to minimize the spread in the fit of $\tilde{m}_0(T,\theta)$ to the data at various angles.

The ellipsometry data were also taken at a single angle, namely the Brewster angle $\theta_1=\theta_B(T)$. The advantage of using $\theta_B(T)$ seems to be mainly conceptual, since the coefficient of ellipticity then has the simple form (1.11). On the other hand, the practical advantages of using a *fixed* incident angle in place of $\theta_B(T)$ are substantial. Thus, experimental use of a fixed angle would eliminate uncertainties incurred in readjusting the angle at each temperature. Likewise, it would reduce uncertainty in and simplify the interpretation of the data. In our calculations, θ_B must first be calculated for each T; this estimate is then used to calculate the desired $\bar{\rho}_B$. Clearly, the calculations would be simpler and more reliable if a single angle were supplied at the start. It should be mentioned, however, that this advantage is mainly technical since $\bar{\rho}$ proves to be fairly insensitive to θ_1 near the Brewster angle. Nevertheless, there would be a significant advantage to using a *series* of fixed angles, as suggested for the reflectivity experiments. Such additional data would provide a useful cross-check of the analysis and help discriminate more reliably between different model profiles. An alternative way to probe different length scales would be to use different wavelengths of incident light.

A further useful improvement in both the reflectivity and ellipsometry experiments would be a more accurate, independent determination of T_c. As seen in Secs. II D and III D, a shift of only one or two millikelvin makes a significant difference in the shape of $\tilde{m}_0(t)$. Since the reduced temperatures are quite small, this is not too surprising. It implies, however, that not only the determination T_c, but also the temperature stability, temperature gradients across the sample cell, and T_c drifts, should be controlled to within a millikelvin if the observed data are to be theoretically useful.

As mentioned in Sec. III A, the data of Schmidt were taken at equilibrium.[8] Schmidt and Moldover, on the other hand, used finite cooling rates: according to their Fig. 6, data were taken at the two rates, 30 mK/h and 5 mK/h. Slower cooling yielded ellipticity coefficients lower by roughly $\Delta\bar{\rho}=3\times10^{-4}$. It was not clear whether $\Delta\bar{\rho}$ was also temperature dependent. If so, the finite cool-

ing rate could have a strong effect on the analysis. Since data taken at the two cooling rates differ significantly, it is clearly preferable to use equilibrium conditions.

Our analysis of the ellipsometry data also revealed a sensitive dependence on the value of the correlation length amplitude ξ_0. A more reliable determination of this quantity, perhaps based on turbidity or scattering measurements taken on the same sample, would be worthwhile in reducing the uncertainty of the analysis.

Finally, we remark that the differences in the reflectivity (or coefficient of ellipticity, by the same token) predicted by different profiles become more pronounced near the critical point; the current data extend down to $t \simeq 10^{-5}$, which is remarkably good experimentally, but closer still would be even more desirable!

B. Additional concerns

In our analysis we have neglected two effects which are potentially relevant, namely, van der Waals forces and critical opalescence: both were discussed briefly in Sec. I F. Here we consider the possible effects of long-range forces on our analysis in a little more detail. van der Waals forces, which are inevitably present in liquids, give rise to a z^{-3} power-law tail in the adsorption profile, which, at sufficiently large z, must dominate the exponential tail which our analysis entails. In order to estimate the significance of van der Waals forces, we may compare the power-law tail directly due to such forces to the exponential adsorption tail arising from the short-range interactions. Specifically, we may suppose the profile due to van der Waals interactions will have the form

$$\delta m(z) \approx \tilde{W}/z^3 \quad \text{as } z \to \infty \ , \tag{4.1}$$

where we neglect retardation effects (since they only *reduce* the magnitude of the van der Waals interactions). The amplitude $\tilde{W}$ should be proportional to the usual Hamaker constant W. If we equate (4.1) to the scaled adsorption profile (1.3) in the region of large $x = z/\xi$, using (1.6), we obtain the equation

$$x^3 e^{-x} = \tilde{C} t^{\beta} \tag{4.2}$$

with $\tilde{C}$ proportional to $\tilde{W}/m_0 P_{\infty}$. If $x = x_{\times} > 1$ is the solution of this equation, the van der Waals induced profile dominates the exponential profile *only* for $z_{\times} > x_{\times} \xi$. To estimate $\tilde{W}$ we argue that for slowly varying external potentials $U(\mathbf{r})$, one has

$$\delta m(\mathbf{r}) \simeq \tilde{\chi} U(\mathbf{r})/k_B T \ , \tag{4.3}$$

where $\tilde{\chi} \propto \chi \approx C^+/t^{\gamma}$ is the appropriate reduced susceptibility. With the aid of hyperscaling relations, C^+ can be related to ξ_0 and the critical amplitude B of the coexistence curve;[39] the magnitude of $U(r)$ follows from the intermolecular van der Waals forces. More detailed arguments are presented in the Appendix; using calculations of Kayser[40] for wetting of a glass substrate in the nitromethane-carbon disulfide mixture and the typical values $m_0 \simeq 1$ and $P_{\infty} \simeq 0.85$, we have estimated $\tilde{C}$ for that mixture as about 0.12. One then finds that the crossover point $x_{\times}$ varies almost linearly with $\log t$ from about 10.8 to 13.8 as t ranges from 0.01 to 10^{-5}. This is an encouraging result since it indicates that $z_{\times}$ is much larger than ξ, well justifying the neglect of van der Waals forces. Even if $\tilde{C}$ were ten times larger, $x_{\times}$ would still exceed 7 to $t < 0.01$. Consequently, we suspect that the neglect of van der Waals forces is also justified in the i-P+pFMCH and MCH+pFMCH mixtures. Other long-range forces, such as those arising from an electric double layer, have also been proposed for insulating binary liquid mixtures in contact with glass,[41,42] but we have not attempted to estimate their possible influence.

C. Concluding remark

In conclusion, we have shown how optical data for critical adsorption from binary liquid mixtures onto a solid wall or vapor interface can be analyzed in a systematic way to check the basic scaling theories and to elucidate the form of the universal scaling function $P(x)$. Existing reflectivity and ellipsometry experiments confirm several important features of $P(x)$ and provide some more detailed quantitative information about the nature of the scaling function. Although the precision and reliability of our present estimates are somwhat limited, future experiments which take appropriate precautions, some emphasized by our analysis, should be able to provide a reasonably accurate view of the scaling function and, consequently, to pose a welcome challenge to theory.

ACKNOWLEDGMENTS

We especially thank Benjamin Widom and Michael R. Moldover, whose encouragement and suggestions were instrumental in our decision to complete and extend this work for publication. We are indebted to Carl Franck, Mark Schlossman, and Xiao-lun Wu, and to James W. Schmidt and Michael R. Moldover for giving us their original data, and are especially grateful to Dr. Schmidt for performing a new experiment and allowing us to analyze his data prior to publication. We have benefited greatly from numerous conversations with Dr. Wu and Dr. Schmidt regarding their experiments. In addition, the interest, advice and aid of Douglas J. Durian and Martin P. Gelfand have been much appreciated; thanks for assistance are also due to Jan V. Sengers, Robert W. Gammon, Paul J. Upton, and Daniel Beysens. We thank Gerhard H. Findenegg and David Beaglehole for their interest in our work. The support of the National Science Foundation, through the Condensed Matter Theory Program, Grant No. DMR 87-01223/96299, and, for A.J.L., through the Graduate Fellowship Program, is gratefully acknowledged.

APPENDIX: EFFECT OF van der WAALS FORCES ON THE ADSORPTION PROFILE

We present here the calculation sketched in Sec. IV B which aims at estimating the effects of van der Waals interactions. The full response to a position-dependent external potential is complicated and nonlocal. The approximation of replacing the nonlocal resonse by a local response leads directly to (4.2). We first present argu-

ments to justify this approximation, and then proceed to estimate the quantities $\tilde{\chi}$ and $U(\mathbf{r})$ in (4.3) which are needed to obtain the crucial constant $\tilde{C}$ in (4.2).

In order to calculate the response of a semi-infinite system to an external potential, consider the partition function. For consistency, we will adopt units of mass density ρ throughout; then one has

$$Z=\mathrm{Tr}_{\rho(\mathbf{r})}\{\exp[(-\mathcal{H}_0[\rho(\mathbf{r})] - \int U(\mathbf{r})\rho(\mathbf{r})d\mathbf{r})/k_BT]\}\ , \tag{A1}$$

where $U(\mathbf{r})$ denotes the external potential energy. For van der Waals forces, this assumes the form

$$U(\mathbf{r})=W^*/z^3\ , \tag{A2}$$

where z measures the distance from the wall bounding the system; the Hamiltonian $\mathcal{H}_0$ contains all the interactions which give rise to the critical adsorption profile (1.3). The response to $U(\mathbf{r})$ is measured by the deviation of the local mean mass density $\langle\rho(\mathbf{r})\rangle$; to first order, one has just

$$\delta\rho(\mathbf{r})=-\beta\int U(\mathbf{r}')[\langle\rho(\mathbf{r})\rho(\mathbf{r}')\rangle_0 - \langle\rho(\mathbf{r})\rangle_0\langle\rho(\mathbf{r}')\rangle_0]d\mathbf{r}'\ , \tag{A3}$$

where the notation $\langle\cdots\rangle_0$ denotes thermal averages taken with respect to $\mathcal{H}_0$. If $U(\mathbf{r})$ is slowly varying on the scale of the bulk correlation length ξ, it can be factored out of the integral. Moreover, if the variation of the correlation functions owing to the presence of the wall is neglected, the remaining integral becomes the reduced bulk susceptibility χ implied by $\mathcal{H}_0$. The response thus simplifies to

$$\delta\rho(\mathbf{r})\simeq-\chi\beta U(\mathbf{r})\ . \tag{A4}$$

By comparing this to (4.1) when $U(\mathbf{r})$ is given by (A2), we find that the desired profile amplitude in (4.1) is

$$\tilde{W}\simeq-\chi W^*/k_BT_c\ . \tag{A5}$$

In order to estimate this, we must determine the susceptibility χ and the strength W^* of the van der Waals potential.

Consider, first, the susceptibility. Asymptotically close to the critical point, one has

$$\chi\approx C^+t^{-\gamma}\ . \tag{A6}$$

The amplitude C^+ can be estimated from the coexistence curve amplitude and correlation length amplitude *via* universal and hyperuniversal amplitude ratios. The coexistence curve of nitromethane-carbon disulfide was measured by Gopal, *et al.*[43] and later reanalyzed by Greer,[44] in terms of the volume fraction of carbon disulfide. Kayser[40] converted Greer's results into units of mass density, and obtained for the mass density difference between the two phases *below* T_c, with $\Delta\rho\approx B_\rho|t|^\beta$,

$$B_\rho\simeq0.278\ \mathrm{g/cm^3}\ . \tag{A7}$$

Now the relevant hyperuniversal amplitude ratio is

$$C^+/B_\rho^2\xi_0^3\equiv Q_\chi^+=3.09\pm0.08\ , \tag{A8}$$

where the value quoted follows from a recent reassessment by Liu and Fisher[39] of amplitude ratios for the three-dimensional Ising model. Consequently, we obtain

$$C^+=0.239\ \xi_0^3\ \mathrm{g^2/cm^6}\ . \tag{A9}$$

(It transpires that the correlation length amplitude ξ_0 cancels out.)

In order to estimate W^*, we appeal to a calculation by Kayser[40] for nitromethane-carbon disulfide in contact with glass. Kayser estimated the force per unit area $F(d)$ due to van der Waals interactions on a wetting layer of the nitromethane-rich phase of thickness d, separating the carbon disulfide-rich phase from a glass substrate. His results for $J(t,d)\equiv F(d)d^3/\Delta\rho g$, where $\Delta\rho$ is the mass density difference between the two phases following from (A7), and g is the acceleration due to gravity, are listed in Table IV of his paper.[40] As an upper bound, we have taken the value $J=5\times10^{-18}\ \mathrm{cm^4}$.

If one models the situation by pairwise additive van der Waals forces, W^* in (A2) is found to be given by

$$W^*\simeq Jg\ . \tag{A10}$$

(It may be noted, however, that Kayser's calculation of J was based on DLP theory[25] and so implicitly includes many-body forces.)

Substituting (A6) and (A10) into (A5) gives, for the amplitude of the van der Waals induced profile,

$$\tilde{W}\simeq-t^{-\gamma}C^+Jg/k_BT_c\ , \tag{A11}$$

where C^+ is given in (A9).

The last step is to compare the van der Waals increment $\delta\rho(z)$ to the critical adsorption profile obtained from fits to the data in Sec. II. According to (1.18), (1.3), and (1.6), the dielectric constant profile for large z is

$$\Delta\epsilon(z)\approx t^\beta m_0P_\infty e^{-z/\xi}\ . \tag{A12}$$

For the purposes of this calculation, we adopt the typical fitted values $m_0=1.0$ and $P_\infty=0.85$.

The dielectric constant profile can be converted into a volume fraction profile using the Lorentz-Lorenz factor $\epsilon_0\simeq0.68$.[22] The volume fraction profile can be converted, in turn, into a number density profile using the definition of volume fraction given below (1.1) in Sec. I. Finally, the number density profile can be converted to a mass density profile by multiplying by B_ρ/B, where B_ρ is given in (A7) while B is the amplitude of the number density curve. The final result is

$$\delta\rho(z)=c_\rho P_\infty B_\rho t^\beta e^{-z/\xi}\ , \tag{A13}$$

where $c_\rho=0.90$ embodies the conversion from dielectric constant to mass density.

Our aim now is to estimate $x_\times=z_\times/\xi$, at which point the induced van der Waals increment matches the exponential adsorption profile. If we equate (A13) to (4.1) with $\tilde{W}$ specified by (A11), we obtain the equation

$$x^3e^{-x}=\tilde{C}t^\beta\ ; \tag{A14}$$

with solution $x_\times$, as already quoted in (4.2). However, we have the explicit expression

$$\tilde{C}=\frac{C^{+}Jg}{c_{\rho}P_{\infty}B_{\rho}k_{B}T_{c}\xi_{0}^{3}}=\frac{Q_{\chi}^{+}B_{\rho}Jg}{c_{\rho}P_{\infty}k_{B}T_{c}}\simeq 0.12\ , \qquad \text{(A15)}$$

where (A9) has been used. This estimate of $\tilde{C}$ may be employed in (A14) to solve for $x_{\times}$. Note that $x_{\times}$ depends only logarithmically on $\tilde{C}$, so it is not necessary to estimate $\tilde{C}$ very accurately. Since $x_{\times}$ turns out to be quite large, the approximations embodied in (A4) prove well justified.

*Present address: Exxon Research and Engineering Co., Annandale, New Jersey 08801.

[1]M. E. Fisher and P.-G. de Gennes, C. R. Acad. Sci. Ser. B **287**, 207 (1978).

[2]The expectation that the profile should decay exponentially, far from the surface, follows from the assumption of short-ranged interactions. In the cases where long-ranged van der Waals interactions are present, the tail should actually decay as a power law rather than as an exponential. This complication will be discussed in greater detail in Sec. IV B and the Appendix.

[3]R. Z. Bariev, Teor. Mat. Fiz. **77**, 127 (1988); **40**, 95 (1979).

[4]M. E. Fisher and J.-H. Chen, J. Phys. (Paris) **46**, 1645 (1985).

[5]H. B. Tarko and M. E. Fisher, Phys. Rev. B **11**, 1217 (1975).

[6]M. Schlossman, X.-l. Wu, and C. Franck, Phys. Rev. B **31**, 1478 (1985).

[7]J. W. Schmidt and M. R. Moldover, J. Chem. Phys. **83**, 1829 (1985).

[8]J. W. Schmidt, Phys. Rev. A (to be published). After the completion of the analysis presented here, the thermometers used in the experiments were recalibrated by Schmidt against an absolute scale, so the temperatures quoted here should be shifted upwards by 0.301 K. This uniform shift has a negligible effect on the reduced temperatures which enter our analysis. In addition, however, the estimate of T_c for the MCH+*p*FMCH mixture has been revised upwards by 5 mK relative to the other temperature data points. This shift does have a significant effect on the reduced temperatures; our proposed profiles now provide a better fit to the data. See Sec. III D for further details.

[9]The adequacy of this approximation is open to question. The bulk refractive index varies with temperature, even at fixed composition, and is in fact very weakly singular at criticality; see (a) G. Stell and J. S. Høye, Phys. Rev. Lett. **33**, 1268 (1974); (b) J. V. Sengers, D. Bedeaux, P. Mazur, and S. C. Greer, Physica A **104**, 573 (1980). Furthermore, since the composition also varies through the profile, these effects will vary with the distance from the substrate. However, it is reasonable to expect that the deviations from the Lorentz-Lorenz relation due to the volume change on mixing and cooperative effects will not be too serious. Nonetheless, it must be recognized that the "profile" determined by the optical data is not strictly proportional to the actual composition profile.

[10]D. Beysens and S. Leibler, J. Phys. (Paris) Lett. **43**, L133 (1982).

[11]G. H. Findenegg and R. Löring, J. Chem. Phys. **81**, 3270 (1984).

[12]S. Blümel and G. H. Findenegg, Phys. Rev. Lett. **54**, 447 (1985).

[13]C. Franck and S. E. Schnatterly, Phys. Rev. Lett. **48**, 763 (1982); J. Dixon, M. Schlossman, X.-l. Wu, and C. Franck, Phys. Rev. B **31**, 1509 (1985).

[14]D. Beaglehole, J. Chem. Phys. **73**, 3366 (1980); **75**, 1544 (1981).

[15]B. Heidel and G. H. Findenegg, J. Chem. Phys. **87**, 706 1987; R. Süssman and G. H. Findenegg, Physica A **156**, 114 (1989).

[16]J. W. Schmidt, J. Chem. Phys. **85**, 3631 (1986).

[17]G. Zalczer, J. Phys. (Paris) **47**, 379 (1986).

[18]A related strategy of analysis was adopted by Zalczer (Ref. 17) to analyze the fluorescence experiment of Beysens and Leibler (Ref. 10). The profile was assumed to be a power law, with the amplitude and exponent of the power law as adjustable parameters. The amplitude was adjusted for each temperature data point, and the deviations of the resulting effective amplitude function from constancy were compared for several guesses of the exponent. Zalczer concluded that $0.3\leq\beta/\nu\leq 0.6$. He also tried the exponential profile, (b) in Sec. I D, and concluded that it too was consistent with the data so that he could *not* establish the existence of a power-law part of the profile. Our analysis is basically orthogonal; we have regarded the exponent of the power law as known and studied the crossover from power law to exponential behavior, while Zalczer assumed a power law and fitted the exponent. We can show that a profile with a power-law piece is preferred by the reflectivity and ellipsometry data.

[19]See, e.g., R. B. Griffiths, in *Phase Transitions and Critical Phenomena*, edited by C. Domb and M. S. Green (Academic, New York, 1972), Vol. 1, p. 7 Sec. VI.

[20]L. Peliti and S. Leibler, J. Phys. C **16**, 2635 (1983).

[21]It should be mentioned that Schmidt and Moldover (Ref. 7) and Schmidt (Ref. 16) have used what amounts to an *ad hoc* scaling form in which $P(x)$ switches at $x=\frac{1}{2}$ from a pure exponential decay to a pure power law with $\beta/\nu=\frac{1}{2}$; continuity of $P(x)$ and dP/dx is assured. Apart from the lack of a parameter to modify the scaling function, the abrupt change of form, and discontinuity in d^2P/dx^2, are undesirable.

[22]Note that in (1.18) we have used a *dielectric constant cutoff* ϵ_{β} rather than a *composition cutoff* at $\varphi(z)=1$ (or equivalently, $m(z)=0.601$ for the nitromethane and carbon disulfide mixture). The two cutoffs are equivalent only if $\epsilon_{\infty}-\epsilon_0=\epsilon_{\beta}$. If we accept this as a definition of the Lorentz-Lorenz factor ϵ_0, we find that $\epsilon_0(m=0.601)=0.57$ at $T=T_c$ for the nitromethane and carbon disulfide mixture. However, SWF (Ref. 6) calculate the Lorentz-Lorenz factor for small deviations from the bulk critical composition $m(z)=0$ for the same mixture; they quote $\epsilon_0(m=0)=0.77$, although by similar arguments we would estimate 0.68. It appears that ϵ_0 is rather strongly *composition dependent* so that the composition profile is not strictly proportional to the dielectric constant profile. The optical experiments we have examined actually probe the latter. For this reason, we have consistently used the form (1.18) with a dielectric constant cutoff and have absorbed ϵ_0 into the amplitude m_0.

One way in which the dielectric constant profiles may be roughly translated into composition profiles is by using a

composition-dependent Lorentz-Lorenz factor which interpolates linearly between $\epsilon_0(m=0)=0.77$ or 0.68 and $\epsilon_0(m=0.601)=0.57$. We have, for our own purposes, prepared some plots of composition profiles this way. However, at a deeper level the question touches directly on the issue of the "true order parameter" for the mixture, which will be some *nonlinear* function of composition deviation *or*, equivalently, of dielectric-constant deviation. One cannot hope to elucidate the point much further with typical experimental data and the current absence of detailed theoretical guidance.

[23]See, e.g., K. Binder, in *Phase Transition and Critical Phenomena,* edited by C. Domb and J. L. Lebowitz (Academic, New York, 1983), Vol. 8, p. 1.

[24]H. Nakanishi and M. E. Fisher, J. Phys. C **16**, L95 (1983); J. Chem. Phys. **78**, 3279 (1983).

[25]I. E. Dzyaloshinskii, E. M. Lifshitz, and L. P. Pitaevskii, Zh. Eksp. Teor. Fiz. **37**, 229 (1960) [Sov. Phys.–JETP **10**, 161 (1960)].

[26]D. Beaglehole, in *Fluid Interfacial Phenomena,* edited by C. A. Croxton (Wiley, New York, 1986), p. 523.

[27]S. Fisk and B. Widom, J. Chem. Phys. **50**, 3219 (1969).

[28]S. Dietrich and R. Schack, Phys. Rev. Lett. **58**, 140 (1987).

[29]D. Bedeaux, E. M. Blokhuis, and J. W. Schmidt, Intl. J. Thermophysics (to be published).

[30]X.-l. Wu, private communication and Ph. D. thesis, Cornell University, 1987.

[31]The dielectric constant of glass was reported by SWF as $\epsilon_\gamma=2.304$. Later, Wu (Ref. 30) concluded that a more accurate value was $\epsilon_\gamma=2.2955$. We have adopted this latter value, except when comparing our fits to the background to those of SWF, who used the former estimate. In practice, the shift in ϵ_γ makes little numerical difference, provided it is used consistently in fitting both the background reflectivity R_b and the critical reflectivity increment ΔR (see Sec. I B).

[32]M. Born and E. Wolf, *Principles of Optics,* 6th ed. (Pergamon, New York, 1980), p. 51.

[33]W. H. Press, B. P. Flannery, S. A. Teukolsky, and W. T. Vetterling, *Numerical Recipes* (Cambridge University Press, New York, 1986), Chaps. 9 and 15.

[34]C. Franck, see M. Schlossman's Ph.D. thesis, Cornell University, 1987.

[35]D. Stauffer, M. Ferer, and M. Wortis, Phys. Rev. Lett. **29**, 345 (1972).

[36]M. R. Moldover, Phys. Rev. A **31**, 1022 (1985); H. Chaar, M. R. Moldover, and J. W. Schmidt, J. Chem. Phys. **85**, 418 (1986).

[37]J. W. Schmidt and M. R. Moldover, J. Chem. Phys. **79**, 379 (1983); M. R. Moldover and J. W. Schmidt, Physica D **12**, 351 (1984).

[38]R. B. Heady and J. W. Cahn, J. Chem. Phys. **58**, 896 (1973).

[39]A. J. Liu and M. E. Fisher, Physica A **156**, 35 (1989).

[40]R. F. Kayser, Phys. Rev. B **34**, 3254 (1986).

[41]R. F. Kayser, Phys. Rev. Lett. **56**, 1831 (1986).

[42]D. Ripple, X.-l. Wu, and C. Franck, Phys. Rev. B **38**, 9054 (1988).

[43]E. S. R. Gopal, P. Chandra Sekhar, G. Ananthakrishna, R. Ramachandra, and S. V. Subramanyam, Proc. R. Soc. London Ser. A **350**, 91 (1976).

[44]S. C. Greer, Phys. Rev. A **14**, 1770 (1976).